

## Subduction initiation at passive margins: Numerical modeling

K. Nikolaeva,<sup>1</sup> T. V. Gerya,<sup>1,2</sup> and F. O. Marques<sup>1,3</sup>

Received 17 April 2009; revised 31 August 2009; accepted 21 October 2009; published 10 March 2010.

[1] Subduction is a key process for terrestrial plate tectonics, but its initiation is still not entirely understood. In particular, despite the abundance of both passive and active continental margins on Earth, no obvious cases of transition between them have been identified so far. It has been shown that at most passive margins, elastic and frictional forces exceed gravitational instability and ridge-push forces, which precludes subduction initiation. Therefore additional factors are needed to start subduction there. We investigated numerically in two dimensions factors controlling passive margins' stability such as age of the oceanic plate, thickness of the continental lithosphere and crust, and density contrast between subcontinental and suboceanic lithospheric mantles. Our numerical experiments show that three subsequent tectonic regimes can develop at a passive margin: (1) stable margin, (2) overthrusting, and (3) subduction. Transition from stable margin to the overthrusting regime is mainly controlled by ductile strength of the lower continental crust. Further transition from overthrusting to the subduction regime is governed by the ductile strength of the subcontinental lithospheric mantle and its chemical density contrast with the suboceanic lithospheric mantle. Our experiments also demonstrate that the age of the oceanic plate is a factor of secondary importance for subduction initiation and only plays a role if other parameters are of critical values. Favorable conditions for subduction initiation thus correspond to passive margins where chemically buoyant (depleted) continental lithosphere becomes thin and hot (Moho temperature  $>660^{\circ}\text{C}$ ). This situation can be occasionally created by superimposed external processes such as rifting and/or thermal-chemical plume activity.

**Citation:** Nikolaeva, K., T. V. Gerya, and F. O. Marques (2010), Subduction initiation at passive margins: Numerical modeling, *J. Geophys. Res.*, 115, B03406, doi:10.1029/2009JB006549.

### 1. Introduction

[2] Subduction has been discussed since the development of the plate tectonics theory. Although numerous publications were dedicated to it, subduction in many aspects is still an enigmatic process. One question of great interest is how subduction zones are born [Stern, 2002]. Answering this crucial question will, in particular, notably advance our understanding of how and when the unique global dynamic regime governed by plate tectonics started on Earth. The gravitational instability of an old oceanic plate is believed to be the main reason for subduction [Vlaar and Wortel, 1976; G. F. Davies, 1999]. Oceanic lithosphere becomes denser than the underlying asthenosphere within 10–50 Ma after it forms in a mid-ocean ridge owing to the cooling from the surface [Oxburgh and Parmentier, 1977; Cloos, 1993]. However, as was very well posed by McKenzie [1977],

despite the favorable gravitational instability and ridge push, the bending and shear resistance of the lithosphere prevent subduction from arising spontaneously. Consequently, the following question arises: What forces can trigger subduction (besides the negative buoyancy and ridge push)? At least 11 hypotheses have been proposed to answer this question: (1) plate rupture within an oceanic plate or at a passive margin [e.g., McKenzie, 1977; Dickinson and Seely, 1979; Mitchell, 1984; Müeller and Phillips, 1991], (2) reversal of the polarity of an existing subduction zone [e.g., Mitchell, 1984], (3) change of transform faults into trenches [e.g., Uyeda and Ben-Avraham, 1972; Hilde et al., 1977; Karson and Dewey, 1978; Casey and Dewey, 1984], (4) sediment or other topographic loading at passive margins [e.g., Dewey, 1969; Fyfe and Leonardos, 1977; Karig, 1982; Cloetingh et al., 1982; Erickson, 1993; Pascal and Cloetingh, 2009], (5) forced convergence at oceanic fracture zones [e.g., Müeller and Phillips, 1991; Toth and Gurnis, 1998; Doin and Henry, 2001; Hall et al., 2003; Gurnis et al., 2004], (6) tensile decoupling of the continental and oceanic lithosphere due to rifting [Kemp and Stevenson, 1996], (7) Rayleigh-Taylor instability due to a lateral buoyancy contrast within the lithosphere [Niu et al., 2003], (8) addition of water into the lithosphere [Regenauer-Lieb et al., 2001; Van der Lee et al., 2008], (9) spontaneous

<sup>1</sup>Department of Geosciences, Swiss Federal Institute of Technology, Zurich, Switzerland.

<sup>2</sup>Department of Geology, Moscow State University, Moscow, Russia.

<sup>3</sup>Now at Departamento Geologia and Centro de Geofísica, Instituto Infante Dom Luis, Faculdade Ciências, Universidade de Lisboa, Lisbon, Portugal.

**Table 1.** Parameters of Conducted Numerical Experiments

Experiment	Density Contrast (Difference) Between Continental and Oceanic Lithospheric Mantles (kg/m <sup>3</sup> )	Thickness of Continental Plate (km)	Temperature at Base of Continental Lithosphere (°C)	Age of Oceanic Plate (Ma)	Internal Friction Angle of Continental Crust, sin( $\varphi$ )	Pore Fluid Pressure Factor $\lambda$	Thickness of Continental Crust (km)	Temperature at Moho on Continent (°C)
1	0	80	1340	40	0.1	1.0	44	904
2	0	90	1345	40	0.1	1.0	44	807
3	0	100	1350	40	0.1	1.0	44	729
4	0	110	1355	40	0.1	1.0	44	665
5	0	120	1360	40	0.1	1.0	44	612
6	0	130	1365	40	0.1	1.0	44	567
7	0	140	1370	40	0.1	1.0	44	528
8	0	150	1375	40	0.1	1.0	44	495
9	25	80	1340	40	0.1	1.0	44	904
10	25	90	1345	40	0.1	1.0	44	807
11	25	100	1350	40	0.1	1.0	44	729
12	25	110	1355	40	0.1	1.0	44	665
13	25	120	1360	40	0.1	1.0	44	612
14	25	130	1365	40	0.1	1.0	44	567
15	25	140	1370	40	0.1	1.0	44	528
16	25	150	1375	40	0.1	1.0	44	495
17	50	80	1340	40	0.1	1.0	44	904
18	50	90	1345	40	0.1	1.0	44	807
19	50	95	1348	40	0.1	1.0	44	766
20	50	100	1350	40	0.1	1.0	44	729
21	50	105	1353	40	0.1	1.0	44	696
22	50	110	1355	40	0.1	1.0	44	665
23	50	120	1360	40	0.1	1.0	44	612
24	50	140	1370	40	0.1	1.0	44	528
25	50	150	1375	40	0.1	1.0	44	495
26	75	80	1340	40	0.1	1.0	44	904
27	75	90	1345	40	0.1	1.0	44	807
28	75	100	1350	40	0.1	1.0	44	729
29	75	110	1355	40	0.1	1.0	44	665
30	75	120	1360	40	0.1	1.0	44	612
31	100	80	1340	40	0.1	1.0	44	904
32	100	90	1345	40	0.1	1.0	44	807
33	100	100	1350	40	0.1	1.0	44	729
34	100	110	1355	40	0.1	1.0	44	665
35	100	120	1360	40	0.1	1.0	44	612
36	100	150	1375	40	0.1	1.0	44	495
37	50	80	1340	20	0.1	1.0	44	904
38	50	90	1345	20	0.1	1.0	44	807
39	50	95	1348	20	0.1	1.0	44	766
40	50	100	1350	20	0.1	1.0	44	729
41	50	105	1353	20	0.1	1.0	44	696
42	50	110	1355	20	0.1	1.0	44	665
43	50	120	1360	20	0.1	1.0	44	612
44	50	80	1340	60	0.1	1.0	44	904
45	50	90	1345	60	0.1	1.0	44	807
46	50	95	1348	60	0.1	1.0	44	766
47	50	100	1350	60	0.1	1.0	44	729
48	50	105	1353	60	0.1	1.0	44	696
49	50	110	1355	60	0.1	1.0	44	665
50	50	120	1360	60	0.1	1.0	44	612
51	50	80	1340	80	0.1	1.0	44	904
52	50	90	1345	80	0.1	1.0	44	807
53	50	100	1350	80	0.1	1.0	44	729
54	50	105	1353	80	0.1	1.0	44	696
55	50	110	1355	80	0.1	1.0	44	665
56	50	120	1360	80	0.1	1.0	44	612
57	50	100	1350	90	0.1	1.0	44	729
58	50	105	1353	90	0.1	1.0	44	696
59	50	110	1355	90	0.1	1.0	44	665
60	25	70	1335	40	0.1	1.0	40	953
61	25	70	1335	40	0.1	1.0	35	858
62	25	70	1335	40	0.1	1.0	30	763
63	25	80	1340	40	0.1	1.0	40	837
64	25	80	1340	40	0.1	1.0	35	754
65	25	80	1340	40	0.1	1.0	30	670
66	25	90	1345	40	0.1	1.0	40	747
67	25	90	1345	40	0.1	1.0	35	672

Table 1. (continued)

Experiment	Density Contrast (Difference) Between Continental and Oceanic Lithospheric Mantles (kg/m <sup>3</sup> )	Thickness of Continental Plate (km)	Temperature at Base of Continental Lithosphere (°C)	Age of Oceanic Plate (Ma)	Internal Friction Angle of Continental Crust, sin( $\varphi$ )	Pore Fluid Pressure Factor $\lambda$	Thickness of Continental Crust (km)	Temperature at Moho on Continent (°C)
68	25	90	1345	40	0.1	1.0	30	598
69	25	100	1350	40	0.1	1.0	40	675
70	25	100	1350	40	0.1	1.0	35	607
71	25	110	1355	40	0.1	1.0	35	554
72	50	60	1330	40	0.1	1.0	30	887
73	50	70	1335	40	0.1	1.0	35	858
74	50	70	1335	40	0.1	1.0	30	763
75	50	80	1340	40	0.1	1.0	40	837
76	50	80	1340	40	0.1	1.0	35	754
77	50	90	1345	40	0.1	1.0	40	747
78	50	95	1348	40	0.1	1.0	35	638
79	50	105	1353	40	0.1	1.0	40	644
80	50	105	1353	40	0.1	1.0	35	580
81	50	105	1353	40	0.1	1.0	30	515
82	50	110	1355	40	0.1	1.0	35	554
83	50	110	1355	40	0.1	1.0	30	493
84	20	70	1335	40	0.1	1.0	40	954
85	20	70	1335	40	0.1	1.0	35	858
86	20	80	1340	40	0.1	1.0	40	837
87	20	80	1340	40	0.1	1.0	35	754
88	20	90	1345	40	0.1	1.0	44	807
89	20	90	1345	40	0.1	1.0	40	747
90	0	100	1350	40	0.2	1.0	44	729
91	25	90	1345	40	0.4	1.0	44	807
92	25	90	1345	40	0.6	1.0	44	807
93	25	100	1350	40	0.4	1.0	44	729
94	25	100	1350	40	0.6	1.0	44	729
95	25	110	1355	40	0.2	1.0	44	665
96	25	110	1355	40	0.3	1.0	44	665
97	25	110	1355	40	0.4	1.0	44	665
98	25	110	1355	40	0.6	1.0	44	665
99	50	90	1345	40	0.4	1.0	44	807
100	50	95	1348	40	0.2	1.0	44	766
101	50	100	1350	40	0.4	1.0	44	729
102	50	105	1353	40	0.2	1.0	44	696
103	50	110	1355	40	0.2	1.0	44	665
104	50	110	1355	40	0.3	1.0	44	665
105	75	100	1350	40	0.4	1.0	44	729
106	75	110	1355	40	0.2	1.0	44	665
107	75	110	1355	40	0.3	1.0	44	665
108	100	90	1345	40	0.4	1.0	44	807
109	100	100	1350	40	0.4	1.0	44	729
110	100	110	1355	40	0.2	1.0	44	665
111	100	110	1355	40	0.3	1.0	44	665
112	100	110	1355	40	0.4	1.0	44	665
113	100	110	1355	40	0.6	1.0	44	665
114	100	120	1360	40	0.2	1.0	44	612
115	100	120	1360	40	0.3	1.0	44	612
116	25	90	1345	40	0.1	0.75	44	807
117	25	90	1345	40	0.1	0.7	44	807
118	25	90	1345	40	0.1	0.6	44	807
119	25	90	1345	40	0.1	0.5	44	807
120	25	110	1355	40	0.1	0.95	44	665
121	100	100	1350	40	0.1	0.75	44	729
122	100	100	1350	40	0.1	0.6	44	729
123	100	100	1350	40	0.1	0.5	44	729
124	100	110	1355	40	0.1	0.75	44	665
125	100	110	1355	40	0.1	0.6	44	665
126 <sup>a</sup>	25	90	1345	40	0.1	1.0	44	807
127 <sup>a</sup>	75	100	1350	40	0.1	1.0	44	729
128 <sup>a</sup>	75	100	1350	40	0.1	1.0	44	729
129 <sup>a</sup>	75	100	1350	40	0.1	1.0	44	729
130 <sup>a</sup>	75	110	1355	40	0.1	1.0	44	665

<sup>a</sup>Experiments with sediment loading; see Table 9.

thrusting of the buoyant continental crust over the oceanic plate [Mart *et al.*, 2005], (10) small-scale convection in the sublithospheric mantle [Solomatov, 2004], and (11) interaction of thermal-chemical plumes with the lithosphere [Ueda *et al.*, 2008].

[3] In the frame of these hypotheses several detailed studies were dedicated to the possible sites of subduction nucleation. It has been shown, for example, that breaking of the mature passive margin is less probable than the lithosphere collapse within the oceanic plate, for example, on transform faults, fracture zones, and spreading ridges [McKenzie, 1977; Müller and Phillips, 1991; Toth and Gurnis, 1998; Hall *et al.*, 2003]. However, passive margins seem to be the logical sites for subduction initiation. The Wilson cycle supposes that the closure of oceanic basins occurs by subduction of the oceanic plate under the continental plate. Indeed, on the Earth nowadays most subduction zones are located along continental margins. One way to account for both an abundance of existing active continental margins and the apparent difficulty of transforming a passive continental margin into an active one is to assume that subduction is triggered by another subduction zone that originated in more favorable conditions [Stern, 2004; Niu *et al.*, 2003]. Existing subduction can lead to development of a new subduction zone either by lateral propagation [Niu *et al.*, 2003] or by weakening another continent-ocean contact, for example, owing to water addition [Van der Lee *et al.*, 2008].

[4] A different way to initiate subduction on passive margins was proposed by Mart *et al.* [2005]. On the basis of the results of analog experiments, these authors suggested that the key factor for subduction generation is a chemical density contrast between continental and oceanic lithospheres. They proposed that the buoyancy contrast within the lithosphere induces secondary extension and compression owing to the tendency of less dense material to “float” and of dense material to “sink,” which leads to the development of reverse (inclined continentward) fault, thus breaking the lithosphere. Recently, Goren *et al.* [2008] supported this conclusion by analytical calculations and additional analog experiments. However, owing to methodological limitations of the analog experiments, the model development has not demonstrated proper one-sided subduction associated with deep sinking of the oceanic slab into asthenospheric mantle but rather showed various overthrusting scenarios when positively buoyant continental lithosphere creeps over the deflecting oceanic plate.

[5] In this paper we elaborate on the ideas of previous workers and test numerically the possibility for triggering proper one-sided subduction at a passive continental margin. By performing systematic 2-D numerical experiments with viscoelastoplastic rock rheology, we investigated the effects of several factors that can control the process of subduction initiation: lithospheric thickness, chemical density contrast between the continental and oceanic lithospheric mantles, age of oceanic plate, and plastic strength and thickness of the continental crust (Table 1). From the numerical results we conclude that density contrast between continental and oceanic lithospheric mantles and ductile strength of the continental lithosphere have a major impact on subduction initiation at passive margins, while the age of

the oceanic plate plays a role only if other parameters are of critical values.

## 2. Model Description

### 2.1. Numerical Implementation

[6] The model is based on the I2ELVIS code [Gerya and Yuen, 2007], which combines conservative finite differences with nondiffusive marker-in-cell techniques. In order to ensure a realistic one-sided [Gerya *et al.*, 2008] subduction pattern, we account for slab dehydration processes on the basis of the Gibbs free energy minimization approach [Connolly, 2005] combined with the moving fluid markers technique [Gerya *et al.*, 2006; Nikolaeva *et al.*, 2008].

[7] In our model we use viscoelastoplastic rheology of the rocks [e.g., Ranalli, 1995]. The plastic strength of a rock is determined as

$$\sigma_{yield} = C + \sin(\varphi)P, \quad (1)$$

$$\sin(\varphi) = \sin(\varphi_{dry})(1 - \lambda), \quad (2)$$

where  $C$  is the cohesion,  $\varphi$  is the effective angle of an internal friction ( $\varphi_{dry}$  is  $\varphi$  for dry rocks),  $P$  is the dynamic pressure, and  $\lambda = P_{fluid}/P$  is the pore fluid pressure factor. For dry crystalline rocks,  $\sin(\varphi)$  typically varies from 0.2 to 0.9, depending on pressure, temperature, and mineralogical composition [Brace and Kohlstedt, 1980; Moore *et al.*, 1997]. Following Gerya *et al.* [2008], we combine high plastic strength of dry mantle ( $\sin(\varphi) = 0.6$ ) and crust ( $\sin(\varphi) = 0.1-0.6$ ) with low plastic strength of hydrated rocks ( $\sin(\varphi) = 0-0.1$ ) forming at the upper interface of the subducting plate in response to oceanic crust dehydration.

### 2.2. Initial and Boundary Conditions

[8] The 2-D model (Figure 1), representing a lithospheric/upper mantle section of a continental margin, is 3000 km wide and 200 km deep. The continental crust consists of two granitic layers of different densities and is 44 km thick in total. The oceanic crust is represented by a 2 km thick upper layer of hydrothermally altered basalts overlying 6 km of gabbroic rocks. The model oceanic crust does not include sediments, but they spontaneously fill the trench after its arcward slope reaches a critical angle of 17°. The mantle sections are modeled as anhydrous peridotite. To investigate the effect of density contrast between continental and oceanic lithospheric mantles, we vary a chemical density of the continental lithospheric mantle, which is known to be generally more depleted than the oceanic lithospheric mantle, from 3200 to 3300 kg/m<sup>3</sup>, and we keep chemical densities of the oceanic lithospheric mantle and the asthenosphere constant and both equal to 3300 kg/m<sup>3</sup> (Table 1). Material properties and chemical composition of each rock type are listed in Tables 2 and 3, respectively.

[9] The initial temperature field for oceanic plate is an oceanic geotherm [Turcotte and Schubert, 2002] for different lithospheric ages (Table 1). In our experiments, composition and flow law for the mantle part of the oceanic lithosphere and for the asthenospheric mantle are taken to be identical (difference in color between them in Figure 1 is

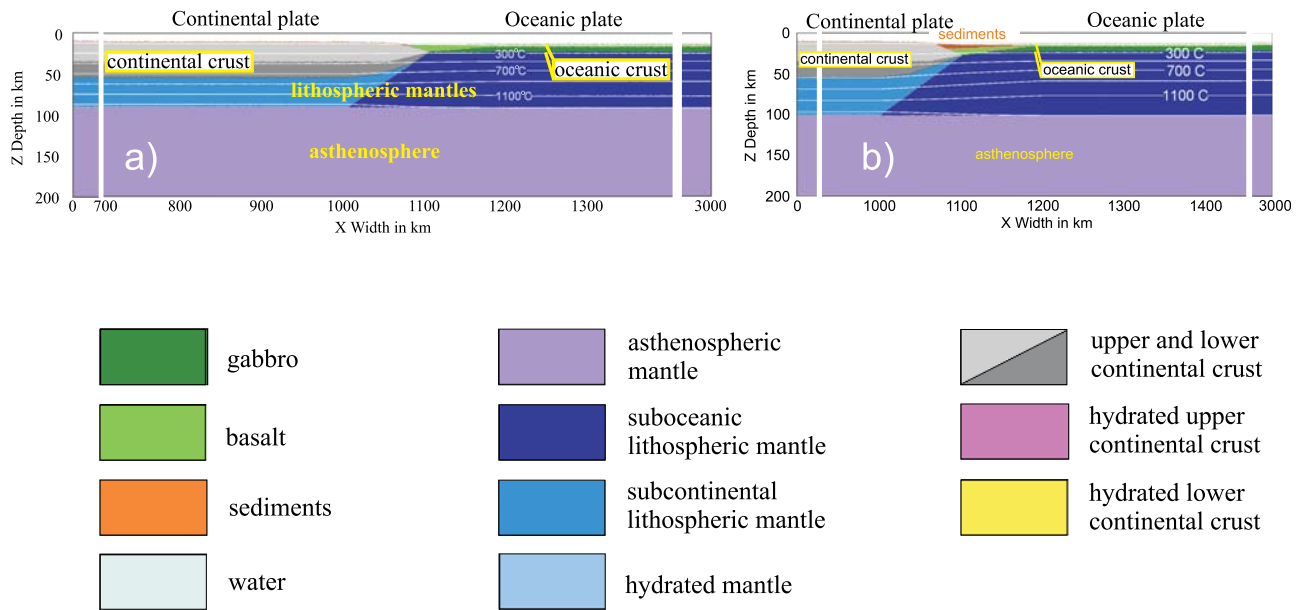


**Figure 1.** Initial configuration of numerical model (a) without sediment loading and (b) with sediment loading (see text for details). Staggered grid resolution:  $801 \times 101$  nodes and 10 million randomly distributed markers. Grid step varies from  $2 \text{ km} \times 2 \text{ km}$  close to the boundary between plates ( $X$  is from 500 to 2400 km) to  $15 \text{ km} \times 2 \text{ km}$  outside of this area. Composition and flow law for the mantle part of the oceanic lithosphere and for the asthenospheric mantle are taken to be identical; the difference in color between them is used for better visualization of slab deformation.

used for better visualization of slab deformation). The actual thickness of the oceanic lithosphere is therefore determined by the imposed temperature structure depending on the cooling age. Temperature structure of the continental plate is controlled by the thickness of the lithosphere and is defined by a linear profile from  $0^\circ\text{C}$  at the surface to a prescribed temperature at the base of the lithosphere (Table 1). The initial temperature gradient in the asthenospheric mantle is  $0.5^\circ\text{C}/\text{km}$ .

[10] The geometry of the model and particularly the ocean-continent transition depicted in Figure 1 are based on the conceptual model of a passive margin generation [e.g., *Whitmarsh et al.*, 2001]. According to this model, the initial rising of the asthenosphere leads to thinning of the overlying lower continental crust before the breakup of the continent. Then the asthenosphere ascends close to the surface, which results in melting, formation of the oceanic lithosphere (including both the crust and the mantle part of the lithosphere), and spreading of the ocean floor. A boundary between two lithospheres is thus inclined toward the continent.

[11] All mechanical boundary conditions are free slip except the lower boundary, which is permeable in the vertical direction. We imposed an internal erosion/sedimentation surface at the top of both plates by using a 10 km thick top layer of “sticky air” with low density ( $1 \text{ kg}/\text{m}^3$ ) and viscosity ( $10^{19} \text{ Pa s}$ ); the oceanic crust is additionally covered by a 4 km thick layer of “sticky sea water” with the density of  $1000 \text{ kg}/\text{m}^3$  and viscosity of  $10^{19} \text{ Pa s}$ . The large viscosity contrasts caused by these low-viscosity boundary layers minimize shear stresses ( $<10^4 \text{ Pa}$ ) at their bottom, and thus the top of the solid portion of the model behaves essentially as a free surface. The validity of the weak layer

approach for approximating the free surface has recently been tested and proven [*Schmeling et al.*, 2008] with the use of a large variety of numerical techniques (including the I2ELVIS code) and comparison with analog modeling. In the model, this internal free surface evolves by erosion and sedimentation as dictated by the transport equation

$$\frac{\partial z_{es}}{\partial t} = v_z - v_x \frac{\partial z_{es}}{\partial x} - v_s + v_e, \quad (3)$$

where  $z_{es}$  is a vertical position of the surface as a function of the horizontal distance  $x$ ;  $v_z$  and  $v_x$  are vertical and horizontal components of the material velocity vector at the surface, respectively; and  $v_s$  and  $v_e$  are sedimentation and erosion rates, respectively, which correspond to the following relations:

$$\begin{aligned} \nu_s &= 0 \text{ mm/yr}, \quad \nu_e = 0.3 \text{ mm/yr}, \quad \text{when } z < 10 \text{ km}, \\ \nu_s &= 0.03 \text{ mm/yr}, \quad \nu_e = 0 \text{ mm/yr}, \quad \text{when } z > 10 \text{ km}, \end{aligned} \quad (4)$$

where  $z = 10 \text{ km}$  is the sea level prescribed in the model. In the proximity of the continental margin, increased effective sedimentation and erosion rates are used, which also account for arcward slope instability.

### 2.3. Water Release and Transport

[12] The model accounts for both water contained in the mineral phases (Table 3) and free pore water contained in sediments and basalts. The equilibrium water content in mineral phases for each lithology is computed as a function of pressure and temperature from an internally consistent

**Table 2.** Material Properties Used in the Numerical Experiments

Material	Thermal Conductivity (W/mK)	Flow Law	Cohesion $C$ (MPa)	Internal Friction, $\sin(\varphi)$
Sediments	$0.64 + [807/(T + 77)]$	wet quartzite	3–10	0.1
Upper oceanic crust	$1.18 + [474/(T + 77)]$	wet quartzite	3–10	0.1
Lower oceanic crust	$1.18 + [474/(T + 77)]$	plagioclase (An <sub>75</sub> )	3	0.2
Continental crust	$0.64 + [807/(T + 77)]$	wet quartzite	3–10	0.1–0.6
Dry mantle	$0.73 + [1293/(T + 77)]$	dry olivine	3	0.6
Hydrated mantle	$0.73 + [1293/(T + 77)]$	wet olivine	3	0.2
References	<i>Clauser and Huenges [1995]</i>	<i>Ranalli [1995]</i>	<i>Ranalli [1995]</i>	<i>Ranalli [1995]</i>

thermodynamic database [Gerya *et al.*, 2006] by free energy minimization [Connolly, 2005]. The content of free water is assumed to decrease linearly with depth:

$$X_{\text{H}_2\text{O}(\rho)}(\text{wt}\%) = X_{\text{H}_2\text{O}(\rho_0)}(1 - 0.02\Delta z), \quad (5)$$

where  $X_{\text{H}_2\text{O}(\rho_0)} = 2$  wt % is the connate water content at the surface and  $\Delta z$  is the depth below the surface (0–50 km). Water released by both dehydration reactions and porous space compaction is assumed to propagate upward until it reaches a rock that can consume an additional amount of water at given temperature and pressure. The upper limit for water content in the mantle wedge is assigned to 2 wt % to account for incomplete hydration due to the channelization of slab-derived fluids [J. H. Davies, 1999]. The velocity of water migration is computed as [Gorczyk *et al.*, 2007]

$$v_{x(\text{water})} = v_x, \quad v_{z(\text{water})} = v_z - v_{z(\text{percolation})}, \quad (6)$$

where  $v_x$  and  $v_z$  are the horizontal and vertical components of the local velocity of the mantle, respectively, and  $v_{z(\text{percolation})} = 0.03$  m/yr is the relative velocity of upward percolation of water through the mantle.

### 3. Numerical Results

[13] In order to investigate factors controlling subduction initiation at passive margins, we carried out around 100

**Table 3.** Model Rock Compositions in Weight Percent<sup>a</sup>

	Sediment	Upper Oceanic Crust	Lower Oceanic Crust	Continental Crust	Mantle
SiO <sub>2</sub>	61.1	47.62	53.49	66.12	45.55
Al <sub>2</sub> O <sub>3</sub>	12.43	14.48	14.07	15.24	4.03
FeO	5.43	10.41	6.86	4.52	7.47
MgO	2.59	6.92	12.07	2.21	37.42
CaO	6.21	13.39	10.73	4.21	3.18
Na <sub>2</sub> O	2.54	2.15	1.22	3.91	0.33
K <sub>2</sub> O	2.13	0.58	0.09	3.38	0.03
H <sub>2</sub> O	7.60	2.78	1.47	2.0	1.98

<sup>a</sup>Sediment is the GLOSS average (global subducted sediment from Plank and Langmuir [1998]). Basalt is an average for the upper 500 m of the igneous section of the oceanic crust [Staudigel *et al.*, 1989]. Gabbro is a synthetic composition for the gabbroic section of the oceanic crust [Behn and Kelemen, 2003], modified to contain up to 1.5 wt % water to represent the effects of lower crustal hydrothermal alteration [Carlson, 2001]. Peridotite is the LOSIMAG composition (low silica magnesium mantle composition with respect to the Ca and Al in chondrites [Morris and Hart, 1986]) chosen to represent mantle peridotite. The compositions have been simplified by the omission of minor elements such as Mn, P, Ti, and Cr and the assumption that all Fe is ferrous; additionally, CO<sub>2</sub> has been removed from the GLOSS sediment composition.

numerical experiments with varying physical parameters (Table 1). The numerical experiments show that three distinct geodynamic regimes can form at a passive margin (Figure 2): (1) stable margin (Figure 2a), (2) overthrusting (Figure 2b), and (3) subduction (Figure 2c). We will now describe tectonic regimes observed in the experiments and then present the effect of each studied parameter on the model development.

### 3.1. Tectonic Regimes

#### 3.1.1. Stable Margin

[14] Strong density contrast between continental crust and adjacent oceanic lithosphere forces continental crust to thrust over the oceanic crust. We term the margin as “stable” when the position of the continent/ocean boundary does not change notably (<30 km) during the entire numerical experiment (>40 Ma). If the plates’ boundary is shifted for more than 30 km, the model is characterized by general overthrusting development.

#### 3.1.2. Overthrusting

[15] Continental crust thrusts over the oceanic plate due to the inherent gravitation instability of the passive margin, where the continental crust lies in contact with the denser

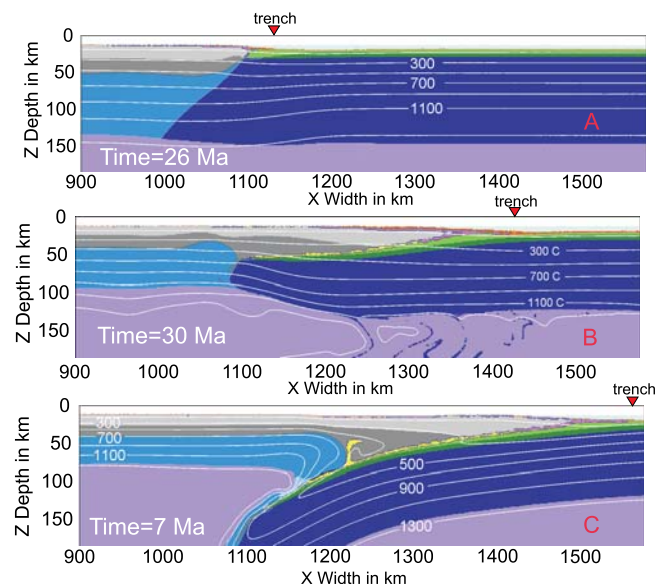


**Figure 2.** Three tectonic regimes observed in the numerical experiments: (a) stable margin (experiment 28, Table 1), (b) overthrusting (experiment 22), and (c) subduction (experiment 6). Color grid is as in Figure 1. Time is dated from the beginning of the experiment.

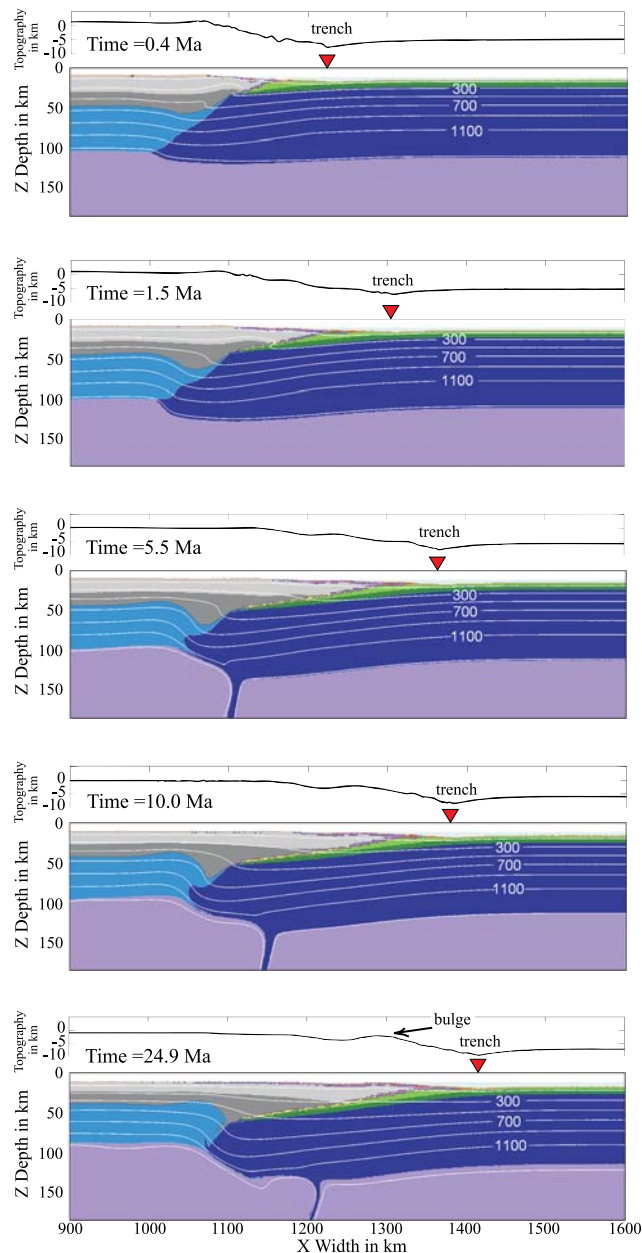


**Figure 3.** Typical overthrusting development (experiment 22). Evolution of lithological and temperature fields with corresponding topography profiles is shown. Continental crust thrusts over the oceanic one. Forming thrust surface is hydrated by water released from the downgoing oceanic crust. The load exerted from shifted continental crust deflects the oceanic plate and causes convective instability at its base (5.5 Ma). The frontal part of the moving continental crust is deflected and forms a bulge at ~120 km from the oceanic trench. Small-scale convection within the asthenospheric mantle induced by instability at the base of the oceanic plate goes on until the end of the experiment, while the overthrusting stops at ~14 Ma.

upper part of the oceanic lithosphere. This results in a thinning of the continental crust at the margin and deflection of the oceanic plate, which indeed remains attached to the continental plate (Figure 3). In this geodynamic regime,

plates are reequilibrated at a new position, which causes convective instability at the base of deflected oceanic lithosphere, producing small-scale convection within the asthenospheric mantle.

### 3.1.3. Subduction

[16] We use the term “subduction” only when there is a breaking of the mantle lithosphere and sinking of spontaneously forming retreating subducting slab overridden by the mantle wedge asthenosphere [Turcotte *et al.*, 1977; Cloos, 1993]. Subduction in the experiments is always preceded by an overthrusting period (Figure 4, 0.3–3.6 Ma) and starts only when stresses at the continent-ocean boundary are high enough to overcome the ductile resistance of the continental mantle lithosphere. Subduction starts by ductile shearing of oceanic-continental mantle boundary driven by stress-sensitive dislocation creep in the mantle. To simplify comparison between different experiments, we determine a conventional time of subduction initiation, which is the time when oceanic crust reaches the depth of 175 km. Timing of subduction initiation differs for different experiments. Two modes of subduction initiation can be distinguished: (1) slow mode, when a significant overthrusting of the continental crust results in a convective instability at the base of the deflected oceanic plate and then (after  $\geq 15$  Ma) is followed by slow sinking of the oceanic lithosphere and initiation of proper subduction (Figure 5), and (2) fast mode, when the overthrusting stage is fast and is immediately followed by sinking of the oceanic plate. Different modes of subduction initiation cause a different initial angle of subduction, which is steeper for slow subduction initiation mode. Experiments generally show different intermediate types of subduction initiation between these end-member modes.

## 3.2. Investigated Parameters

### 3.2.1. Thicknesses of the Continental Crust and the Entire Continental Lithosphere

[17] We carried out experiments with different thicknesses of the continental crust and different thicknesses of the entire continental lithosphere (Tables 4–6) to test the influence of the temperature structure of the continent. Experiments consecutively show transition from fast to slow subduction mode with increasing thickness of the continental lithosphere (from 80 to 100 km; Figure 6), until its critical thickness is reached. After this critical thickness (95–105 km, depending on over parameters) is reached, no subduction occurs, and experiments are characterized by overthrusting tectonic regime (Figures 7 and 8). Experiments with further increasing continental thickness show less amount of overthrusting (Figures 9 and 10), and ultimately only a small part (<30 km) of continental crust is perturbed; thus, we term such a margin as stable. The thickness of continental crust has an opposite effect: that is, thinner continental crust prevents subduction and thus shifts the maximum lithosphere thickness required for subduction initiation (Figure 11 and Table 6).

### 3.2.2. Density Contrast Between Subcontinental and Suboceanic Lithospheric Mantle

[18] We studied the influence of the density contrast between two lithospheric mantles by varying the density of continental lithospheric mantle from 3200 to 3300 kg/m<sup>3</sup> (Table 4). Experiments show that the effect of density contrast is opposite to that of the thickness of the continent

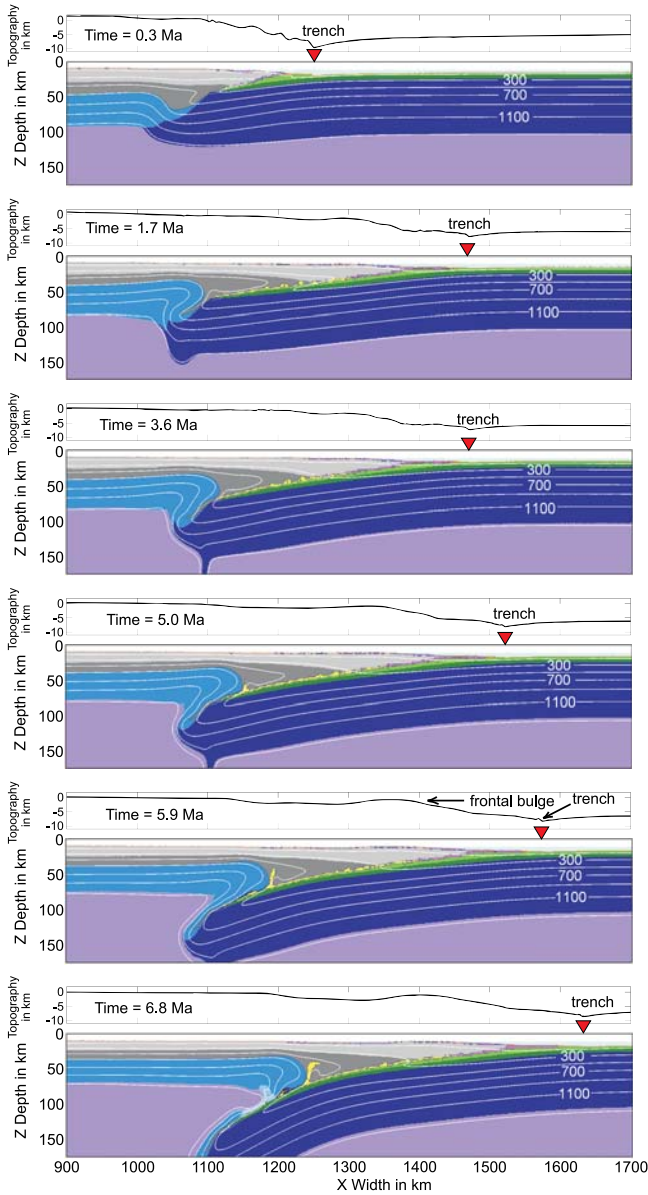


**Figure 4.** Typical subduction initiation development (experiment 28). At the beginning of the experiment, continental crust thrusts over the oceanic one, causing deflection of the oceanic plate, convective instability, and delamination of the oceanic lithospheric mantle (time is 0.3–5 Ma). At ~5 Ma, subcontinental lithospheric mantle starts to shear along the plates’ boundary, and in less than 1 Ma, proper subduction starts. As oceanic plate sinks into the asthenosphere, it releases water and hydrates the overlying continental crust and mantle.

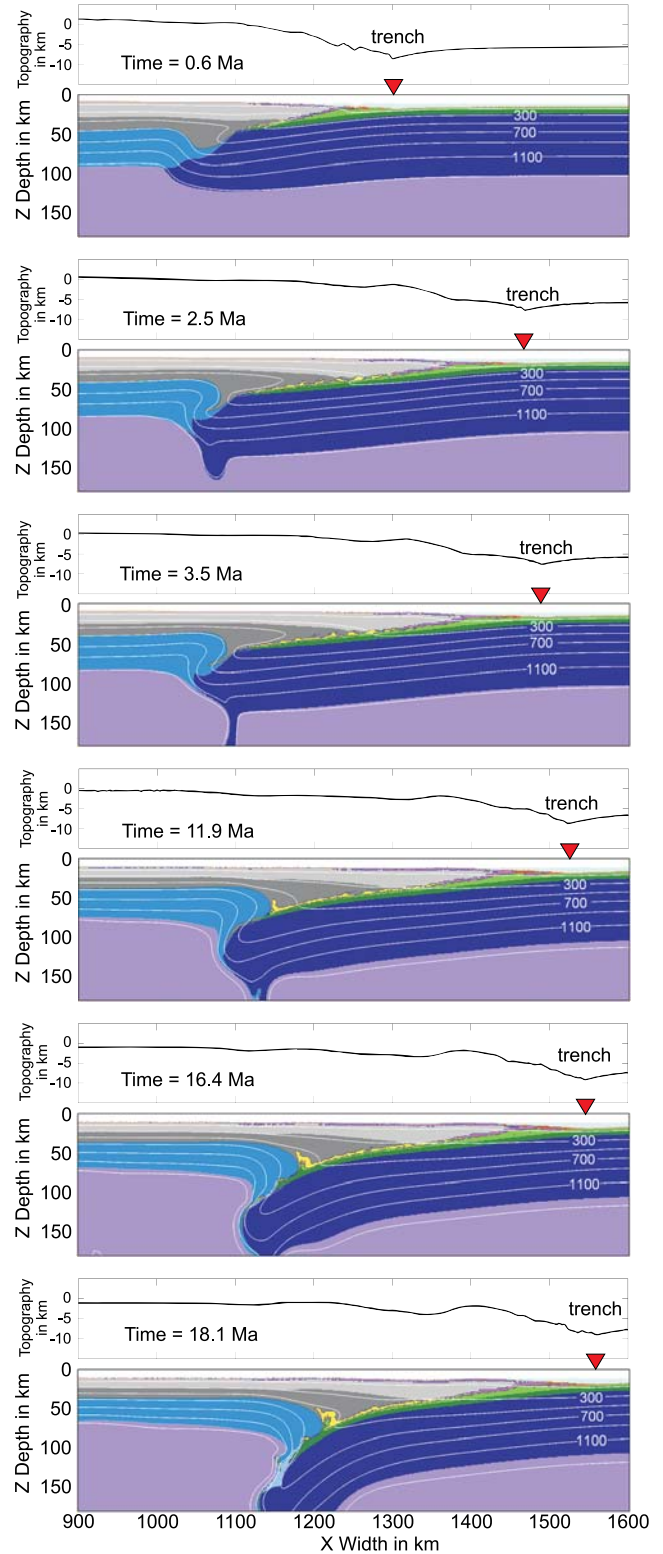


**Figure 5.** Slow mode of subduction initiation (experiment 20). Continental crust thrusts over the oceanic one from the beginning of the experiment, causing oceanic plate deflection and inducing the convective instability at the base of the oceanic lithosphere (time is 2.5 Ma). Subsequent prolonged shear of subcontinental lithospheric mantle ultimately results in the lithosphere failure and subduction initiation (times are 16.4 and 18.1 Ma).

(Figure 7). A larger density contrast favors transition from stable margin to overthrusting tectonic regime or, in the case of auspicious thickness of the continent, transition from overthrusting to subduction development. If the continent is relatively thin and an experiment is characterized by subduction development, then a larger density contrast promotes fast subduction mode; in the case of the overthrusting

**Table 4.** Description of Numerical Experiments 1–36 With Varying Density Contrast Between Subcontinental and Suboceanic Lithospheric Mantle and Thickness of the Continental Lithosphere<sup>a</sup>

Experiment	Density Contrast (kg/m <sup>3</sup> )	Thickness of Continental Plate (km)	Geodynamic Regime	Time of Subduction Initiation (Ma)	Thrust Sheet Length (km)
1	0	80	subduction	1.1	...
2	0	90	subduction	8.4	...
3	0	100	overthrusting	...	250
4	0	110	overthrusting	...	100
5	0	120	stable margin	...	30
6	0	130	stable margin	...	15
7	0	140	stable margin	...	0
8	0	150	stable margin	...	0
9	25	80	subduction	0.8	...
10	25	90	subduction	2.7	...
11	25	100	subduction	34.2	...
12	25	110	overthrusting	...	250
13	25	120	overthrusting	...	110
14	25	130	overthrusting	...	70
15	25	140	stable margin	...	30
16	25	150	stable margin	...	0
17	50	80	subduction	0.7	...
18	50	90	subduction	1.7	...
19	50	95	subduction	5.8	...
20	50	100	subduction	19.4	...
21	50	105	overthrusting	...	350
22	50	110	overthrusting	...	320
23	50	120	overthrusting	...	180
24	50	140	overthrusting	...	85
25	50	150	overthrusting	...	50
26	75	80	subduction	0.7	...
27	75	90	subduction	1.3	...
28	75	100	subduction	6.8	...
29	75	110	overthrusting	...	350
30	75	120	overthrusting	...	280
31	100	80	subduction	0.6	...
32	100	90	subduction	1.2	...
33	100	100	subduction	4.1	...
34	100	110	subduction	20.1	...
35	100	120	overthrusting	...	280
36	100	150	overthrusting	...	110

<sup>a</sup>The age of the oceanic plate is 40 Ma,  $\sin(\varphi)$  of the continental crust equals 0.1, and thickness of the continental crust equals 44 km.

tectonic regime, a larger density contrast supports the formation of a longer thrust sheet (Figure 10b).

### 3.2.3. Age of the Oceanic Plate

[19] Age of the oceanic plate in the experiments was 20, 40, 60, 80, and 90 Ma (Table 5). Its effect on the overthrusting tectonic regime is similar (but less strong) to that of the thickness of the continent: younger (and thus hotter) oceanic lithosphere provides more favorable conditions for formation of a longer thrust sheet (Figures 8 and 10a). The age of the oceanic plate is the factor of secondary importance for the subduction initiation: it only plays a role if other parameters are of critical values (Figures 6 and 8).

### 3.2.4. Plastic Strength of the Continental Crust

[20] To test the influence of the continental crust strength, we carried out experiments with different values of effective internal friction angle for anhydrous crustal rocks, keeping other parameters constant (Table 7). Not surprisingly, stronger crust causes formation of a shorter thrust sheet (Figure 12). On the other hand, influence of the continental crust strength on the subduction initiation process is not so straightforward. General development of the subduction

process in experiments with stronger crust remains the same as that for the reference experiments with  $\sin(\varphi) = 0.1$ , but the time needed for subduction initiation changes depending on the mode of this process (“slow” or “fast”). Stronger crust ( $\sin(\varphi) = 0.2$ – $0.6$ ) increases the initiation time by 0.3–2.5 Ma if other model parameters favor a fast mode of subduction initiation (Figure 13). In contrast, in slow subduction initiation mode, stronger plastic crust speeds up the process by 4–7 Ma (Figure 14).

### 3.2.5. Plastic Strength of Hydrated Rocks

[21] Fluid released from the oceanic crust (owing to either subduction or thrusting of continental crust over the oceanic one) hydrates the overlying lithospheric rocks and weakens the slab interface, which has a crucial role in the development of self-sustained one-sided subduction [Gerya *et al.*, 2008]. In most experiments, we used zero values of friction coefficient for rocks in the presence of fluid [Gerya *et al.*, 2008]. However, most fluids may be dismissed at shallow depth, particularly in the case of prolonged initial overthrusting, leading to increased coupling between plates. To test the possible influences of stronger coupling between plates [e.g., Sobolev and Babeyko, 2005], we ran additional experiments with varying pore fluid pressure factor  $\lambda$ , which is related to the effective friction angle  $\varphi$  through equation (2) (Table 8). Experiments show that increasing friction atop the slab leads to formation of shorter thrust sheets. If experiments showed “fast” subduction development mode, then stronger coupling between plates postpones the initiation of subduction and leads to a steeper angle of slab sinking. In the case of a “slow” mode of subduction initiation, increasing friction

**Table 5.** Description of Numerical Experiments 37–59 With Varying Age of the Oceanic Plate and Thickness of the Continental Lithosphere<sup>a</sup>

Experiment	Age of Oceanic Plate (Ma)	Thickness of Continental Plate (km)	Geodynamic Regime	Time of Subduction Initiation (Ma)	Thrust Sheet Length (km)
37	20	80	subduction	0.6	...
38	20	90	subduction	1.9	...
39	20	95	subduction	10.2	...
40	20	100	overthrusting	...	420
41	20	105	overthrusting	...	370
42	20	110	overthrusting	...	350
43	20	120	overthrusting	...	280
44	60	80	subduction	0.8	...
45	60	90	subduction	2.0	...
46	60	95	subduction	4.0	...
47	60	100	subduction	18.2	...
48	60	105	overthrusting	...	320
49	60	110	overthrusting	...	270
50	60	120	overthrusting	...	150
51	80	80	subduction	0.9	...
52	80	90	subduction	2.2	...
53	80	100	subduction	17.9	...
54	80	105	overthrusting	...	320
55	80	110	overthrusting	...	200
56	80	120	overthrusting	...	140
57	90	100	subduction	18.1	...
58	90	105	subduction	45.1	...
59	90	110	overthrusting	...	200

<sup>a</sup>The density contrast between continental and oceanic lithospheric mantle is  $\Delta\rho = 50$  kg/m<sup>3</sup>, thickness of the continental crust equals 44 km, and  $\sin(\varphi)$  of the continental crust equals 0.1.

**Table 6.** Description of Numerical Experiments 60–89 With Varying Thickness of the Continental Crust<sup>a</sup>

Experiment	Density Contrast (kg/m <sup>3</sup> )	Thickness of Continental Plate (km)	Thickness of Continental Crust (km)	Geodynamic Regime	Time of Subduction Initiation (Ma)	Thrust Sheet Length (km)
60	25	70	40	subduction	0.8	...
61	25	70	35	subduction	5.02	...
62	25	70	30	overthrusting	...	70
9 <sup>b</sup>	25	80	44	subduction	0.8	...
63	25	80	40	subduction	3.3	...
64	25	80	35	overthrusting	...	150
65	25	80	30	stable margin	...	30
10 <sup>b</sup>	25	90	44	subduction	2.7	...
66	25	90	40	overthrusting	...	230
67	25	90	35	overthrusting	...	60
68	25	90	30	stable margin	...	0
11 <sup>b</sup>	25	100	44	subduction	34.2	...
69	25	100	40	overthrusting	...	180
70	25	100	35	stable margin	...	0
12 <sup>b</sup>	25	110	44	overthrusting	...	250
71	25	110	35	stable margin	...	0
72	50	60	30	subduction	20.9	...
73	50	70	35	subduction	4.9	...
74	50	70	30	overthrusting	...	110
75	50	80	40	subduction	1.86	...
76	50	80	35	overthrusting	...	150
18 <sup>b</sup>	50	90	44	subduction	1.7	...
77	50	90	40	subduction	20.4	...
19 <sup>b</sup>	50	95	44	subduction	5.8	...
78	50	95	35	stable margin	...	30
21 <sup>b</sup>	50	105	44	overthrusting	...	350
79	50	105	40	overthrusting	...	100
80	50	105	35	stable margin	...	5
81	50	105	30	stable margin	...	0
22 <sup>b</sup>	50	110	44	overthrusting	...	320
82	50	110	35	stable margin	...	0
83	50	110	30	stable margin	...	0
84	20	70	40	subduction	0.9	...
85	20	70	35	subduction	6.1	...
86	20	80	40	subduction	4.8	...
87	20	80	35	overthrusting	...	180
88	20	90	44	subduction	3.9	...
89	20	90	40	overthrusting	...	280

<sup>a</sup>Thickness of the continental lithosphere, density contrast between suboceanic and subcontinental lithospheric mantles, and age of the oceanic plate are taken from corresponding reference models with the thickness of the continental crust as 44 km (Table 4).

<sup>b</sup>Results of reference experiments with 44 km thick continental crust listed also in Table 4.

between plates leads to the earlier subduction initiation. Our experiments show that concerning the initial stage of subduction, the effect of increasing plastic strength of hydrated rocks is very similar to that of increasing plastic strength of the continental crust only (compare Figures 15 and 16), although a higher strength of hydrated mantle rocks could also play a role in a long-term evolution of the subduction system [Sobolev and Babeyko, 2005; Gerya et al., 2008].

### 3.2.6. Sediment Loading

[22] Another parameter that may control the evolution of passive margins is sediment loading [Cloetingh et al., 1984, 1989; Regenauer-Lieb et al., 2001]. Sediments accumulating at passive margins depress the oceanic plate and thus seem to provide the favorable conditions for further bending of the plate and the lithosphere break off. Therefore we ran a few additional experiments to test the influence of the sediment loading on the passive margin evolution (Table 9). In those experiments, part of the oceanic plate adjacent to the continent was initially deflected, and sediments up to 10 km thick were put on top of it (Figure 1b). Our experiments

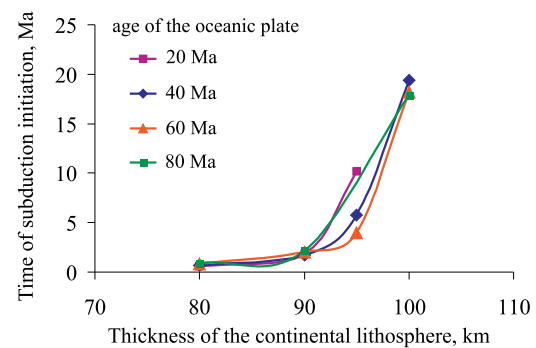


**Figure 6.** Time of subduction initiation as a function of the thickness of the continental lithosphere. Density contrast between suboceanic and subcontinental lithospheric mantles is 50 kg/m<sup>3</sup>. Note that age of the oceanic plate does not notably affect the time for subduction initiation.

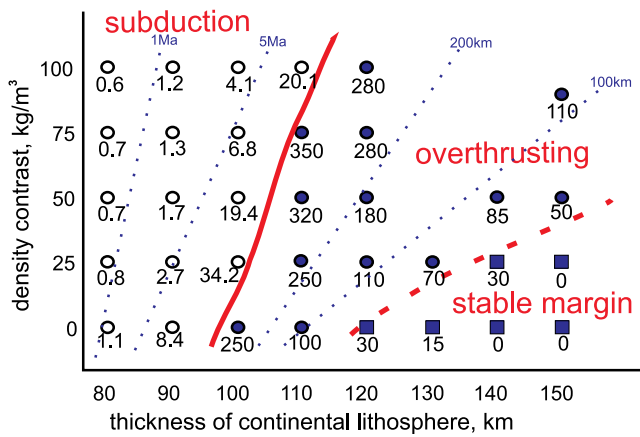


**Figure 7.** Area diagram representing changes of tectonic regime in reference to density contrast between continental and oceanic lithospheric mantle and thickness of the continental lithosphere. Different symbols correspond to different tectonic regimes shown by the numerical experiments: open circles denote subduction, solid circles denote overthrusting, and solid squares denote stable margin. Red lines mark transitions between regimes. Numbers below each symbol indicate either time of subduction initiation in Ma (in the subduction field of the diagram) or the thrust sheet length in kilometers (in the overthrusting and stable margin fields of the diagram). Contour dotted lines of equal time of subduction initiation and of equal length of the thrust sheet are shown in the subduction and overthrusting fields, respectively.

show that sediment loading promotes overthrusting rather than subduction (Table 9).

## 4. Discussion

### 4.1. Factors Controlling Stability of the Passive Margin

[23] Subduction initiation is triggered by gravitational instability of the oceanic plate and is deterred by shear resistance at the plane between subducting and overriding plate. We will now discuss what are the parameters affecting the balance between these two forces, according to presented experimental results.

[24] Subduction is thought to be the consequence of the gravitational instability raised from the oceanic lithosphere aging and cooling. It was generally accepted that the colder, that is, denser, plate sinks into the asthenosphere more readily [Vlaar and Wortel, 1976]. More recent studies have shown that the relationship between density and age of the oceanic lithosphere does not always follow the common half-space cooling model and that the plate does not become significantly denser after 70–100 Ma [e.g., Parsons and Sclater, 1977; Vlaar and Wortel, 1976]. Another complexity added to the initial concept lies in increasing the strength of the plate with increasing age. Particularly, it has seemed to be more difficult to bend older plate and initiate subduction [Cloetingh et al., 1982; Müller and Phillips, 1991]. Together, these findings lead to the conclusion that growing age of the oceanic plate alone does not promote (or even

opposes) subduction initiation. The experimental results showed that the age of the oceanic plate does not determine the tectonic regime on a continental margin, although its minimum value is necessary to obtain gravitationally unstable, negatively buoyant plate (Figures 6 and 8). It is seen from Figure 8 that the transition boundary between subduction initiation and overthrusting regimes is very steep and does not notably depend on the age of the oceanic plate. Indeed, it has been recently demonstrated [Gerya and Yuen, 2007] that even old oceanic plates may be easily bent by pressure-dependent viscoplastic failure promoted by deep penetration of localized normal faults into the slab.

[25] In addition to age of the oceanic plate, sediment loading has been proposed as a factor inducing oceanic plate flexure and thus promoting a plate rupture [Cloetingh et al., 1984, 1989]. This seems not to be supported by our experiments where subduction starts by ductile flexure of the continental lithospheric mantle rather than by brittle/plastic failure of the oceanic plate. Consequently, sediment loading in our experiments promotes overthrusting rather than subduction by preventing the sharp bending of the oceanic plate necessary for the ductile flexure of continental lithospheric mantle.

[26] Shear resistance preventing subduction could be reduced by weakening the plates' boundary, for example, by warming it up or by water addition [e.g., Van der Lee et al., 2008]. One of the main conclusions derived from our experiments is that stability of the passive margin depends mainly on the ductile strength of the continental plate rather than on that of the oceanic plate (Figures 6–8). The strength profiles across the continental margins also consistently

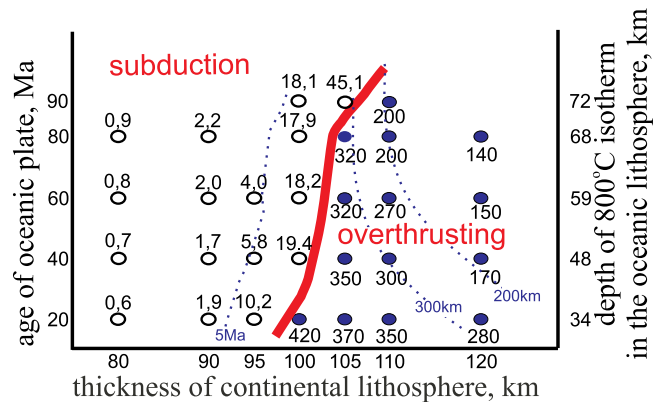


**Figure 8.** Area diagram representing change of tectonic regime in reference to the age of the oceanic plate and thickness of the continental lithosphere. Open circles denote experiments with subduction initiation, and solid circles denote experiments that showed overthrusting. The red line marks the transition between these regimes. Numbers beside each symbol indicate either time of subduction initiation in Ma (in the subduction field of the diagram) or the thrust sheet length in kilometers (in the overthrusting field of the diagram). Contour dotted lines of equal time of subduction initiation (5 Ma) and of equal length of the thrust sheet (200 and 300 km) are shown in the subduction and overthrusting fields, respectively.

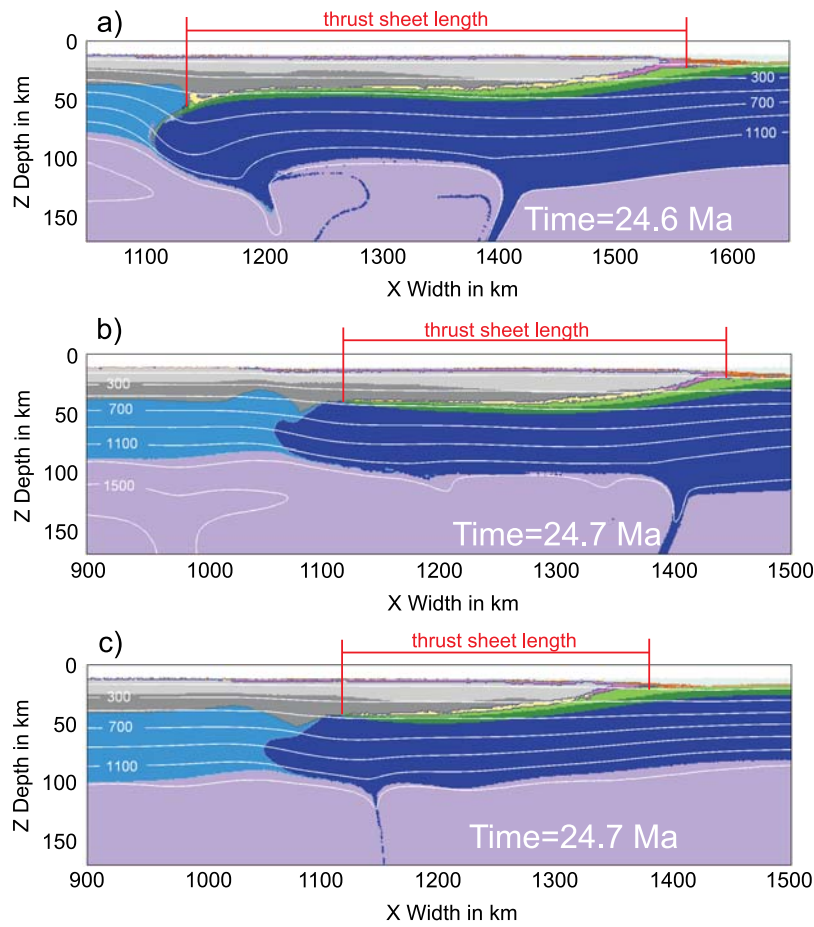


**Figure 9.** Thrust sheet length for experiments with different thicknesses of the continental plate, keeping other model parameters constant: (a) experiment 40 (continental lithosphere thickness equals 100 km), (b) experiment 42 (110 km), and (c) experiment 43 (120 km). The thrust length is measured as the distance from the beginning of the buried oceanic crust to the end of the frontal hydrated part of the continental crust. The length of overthrusting decreases with increasing thickness of the continental lithosphere (from 100 to 120 km) and respectively decreasing Moho temperature (from 630°C to 525°C).

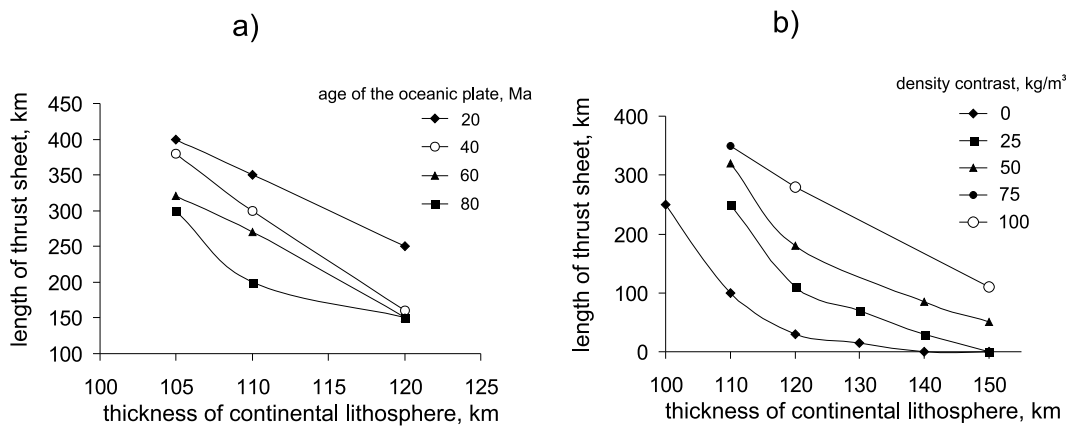


**Figure 10.** Length of thrust sheet as a function of thickness of the continental lithosphere for different (a) age of the oceanic plate (for experiments where density contrast between lithospheric mantles equals 50 kg/m<sup>3</sup>) and (b) density contrast between continental and oceanic lithospheric mantle (for experiments with 40 Ma old oceanic plate).

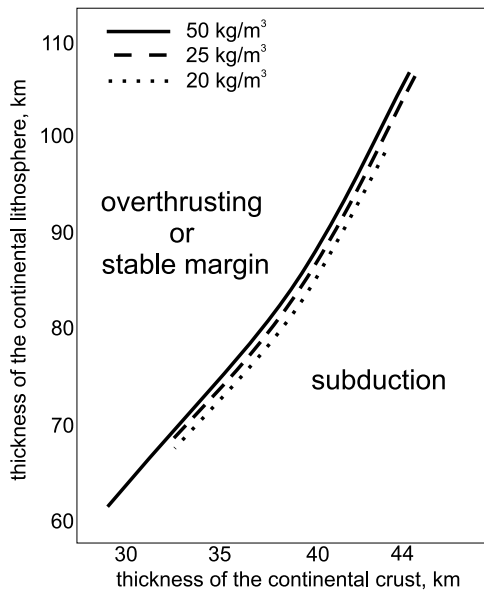


**Figure 11.** Transition from the subduction geodynamic regime to overthrusting and stable margin regimes as a function of both thickness of the continental crust and thickness of the continental lithosphere. Maximum thickness of the continental lithosphere required for successful subduction initiation decreases with decreasing continental crust thickness. Solid, dashed, and dotted lines represent the transition between tectonic regimes shown by experiments with the density contrast between suboceanic and subcontinental lithospheric mantles of  $\Delta\rho = 50$ , 25, and 20  $\text{kg/m}^3$ , respectively.

show the common higher strength on the oceanic side and lower strength landward [Steckler and ten Brink, 1986].

[27] In our models, subduction is started by shearing between continental and oceanic lithospheres and is controlled by both crustal and mantle deformation. Fast and slow modes of subduction initiation observed in our experiments reflect the predominance of one of these factors and thus respond differently on the changing strengths of crustal rocks. The fast mode of subduction initiation depends mainly on the progress of crustal deformation, and consequently, an increase in the strength of the continental crust postpones the development of the subduction zone (Figures 15 and 16). The slow mode of subduction initiation is controlled mostly by the progress of the mantle lithosphere deformation. In this case the increase in strength of the upper (brittle/plastic) crust results in the shorter and thicker thrust sheet, which in turn causes sharper deflection of the oceanic plate downward. Sharper deflection promotes faster growth of stresses in the continental mantle, which speeds up subduction initiation (Figures 15 and 16).

[28] In addition to ductile strength of the continental lithosphere, the compositional density contrast between continental and oceanic lithospheric mantle strongly affects the coherence of the joint lithosphere [Mart *et al.*, 2005]. The results of numerical experiments show that larger density contrast between lithospheric mantles strongly promotes subduction initiation (Figure 7) or provides favorable

conditions for formation of a longer thrust sheet, depending on the strength of the continental lithosphere (Figures 7 and 10b). It is known that typical lithospheric mantle beneath continents is compositionally depleted and thus positively buoyant compared to the ambient mantle, which contributes to the stability of continents [Jordan, 1978; Sankaran, 2001; Carlson *et al.*, 2005]. Density of subcontinental lithospheric mantle is related to its tectonothermal age [Poudjom Djomani *et al.*, 2001; Deen *et al.*, 2006] and thus varies broadly, being lowest ( $\Delta\rho = 80 \text{ kg/m}^3$  with respect to the primitive mantle from Poudjom Djomani *et al.* [2001]) beneath Arcons (i.e., areas experienced their last major tectonothermal event  $>2.5$  Gyr ago) and highest ( $\Delta\rho = 30 \text{ kg/m}^3$ ) beneath Tectons (were modified since 1.0 Ga). From this point of view, passive margins are likely the potential sites for new subduction zones. However, no obvious subduction initiation occurs along passive margins in the Atlantic and Indian Oceans, although it has been proposed by some authors [e.g., Lallemand *et al.*, 2001]. The first reason for this lies in the geological structure of passive margins. They are not abrupt boundaries of continental and oceanic lithosphere. Rather, passive margins represent gradual transitions, which extend over a few hundred kilometers. Moreover, many passive margins are characterized by thick sequences of basalts and intrusions produced by mantle plumes during continental breakup [Eldholm and Coffin, 2000; Stern, 2004]. These magmatic sequences are rheologically strong and difficult to break, and their formation depleted lithospheric roots, making them too buoyant to

**Table 7.** Description of Numerical Experiments 90–115 With Varying Friction Coefficient of the Continental Crust<sup>a</sup>

Experiment	Reference Experiment With $\sin(\varphi) = 0.1$	Internal Friction of Continental Crust, $\sin(\varphi)$	Geodynamic Regime	Time of Subduction Initiation (Ma)	Thrust Sheet Length (km)
90	3	0.2	overthrusting	...	130
91	10	0.4	subduction	3.1	...
92	10	0.6	subduction	3.4	...
93	11	0.4	subduction	26.7	...
94	11	0.6	subduction	18.7	...
95	12	0.2	overthrusting	...	100
96	12	0.3	overthrusting	...	50
97	12	0.4	stable margin	...	15
98	12	0.6	stable margin	...	10
99	18	0.4	subduction	5.1	...
100	19	0.2	subduction	6.5	...
101	20	0.4	subduction	16.5	...
102	21	0.2	subduction	32	...
103	22	0.2	overthrusting	...	205
104	22	0.3	overthrusting	...	150
105	28	0.4	subduction	9.6	...
106	29	0.2	overthrusting	...	300
107	29	0.3	overthrusting	...	250
108	32	0.4	subduction	1.5	...
109	33	0.4	subduction	5.1	...
110	34	0.2	subduction	20.5	...
111	34	0.3	subduction	19.2	...
112	34	0.4	subduction	20.6	...
113	34	0.6	subduction	20.4	...
114	35	0.2	overthrusting	...	250

<sup>a</sup>All other model parameters are taken from the reference experiments with  $\sin(\varphi) = 0.1$  (Table 4).

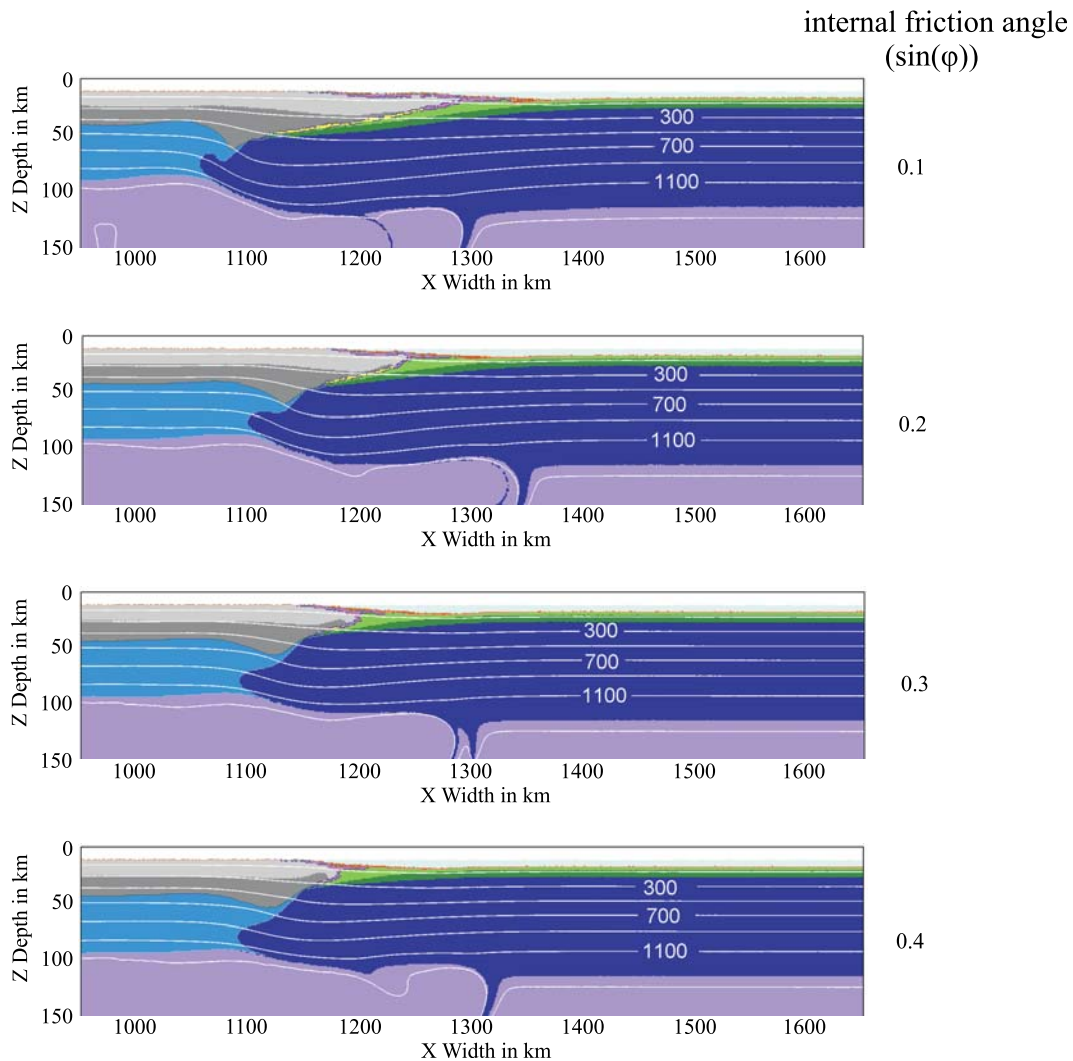


**Figure 12.** Influence of the plastic strength of the continental crust on the overthrusting process. Stronger crust causes formation of shorter thrust sheets (experiments 12, 93, 94, and 95, from top to bottom). Thickness of the continental lithosphere in all experiments was 110 km, age of the oceanic plate was 40 Ma, density contrast between lithospheric mantles was  $25 \text{ kg/m}^3$ , and time was 30 Ma.

sink. The second reason is that in terms of stability of the passive margin, the thickness and degree of depletion of the continental lithospheric mantle are counterinteracting (Figure 7), while in nature these parameters are typically positively correlated [Lee *et al.*, 2001; O'Reilly and Griffin, 2006]. Thus, the density contrast between oceanic mantle lithosphere and rather thin continental lithosphere is likely to be  $\leq 25 \text{ kg/m}^3$  [Sobolev *et al.*, 1997].

[29] To summarize, the model predicts that subduction starts (1) when the negative buoyancy of the oceanic plate is achieved (already from 20 Ma old plate), (2) when the continental lithospheric mantle is rather depleted ( $\Delta\rho \geq 50 \text{ kg/m}^3$ ), and (3) when the Moho temperature in the large region of the continental plate is notably elevated ( $>650^\circ\text{C}$ ), which allows for ductile creep of both the lower continental crust and the lithospheric mantle to be simultaneously activated. Note that such high-temperature conditions may be rarely achieved in nature and limited to special cases of

strongly thinned/weakened (e.g., rifted and/or affected by thermal-chemical plumes) margin lithosphere [Van der Lee *et al.*, 2008].

#### 4.2. Topography Indications

[30] Subduction presented in numerical models is always preceded by thrusting of the continental crust over the oceanic plate owing to the strong density contrast between continental crust and adjacent oceanic lithosphere. We studied topography expressions of each tectonic regime in order to obtain a distinction criterion, potentially applicable to nature.

[31] Both subduction and overthrusting are characterized by the development of an oceanic trench (Figures 3, 4, and 17) with the maximum trench depth varying from 8 to 11 km. Trench formation results from the large initial instability at the margin, which forces intense thrusting of the

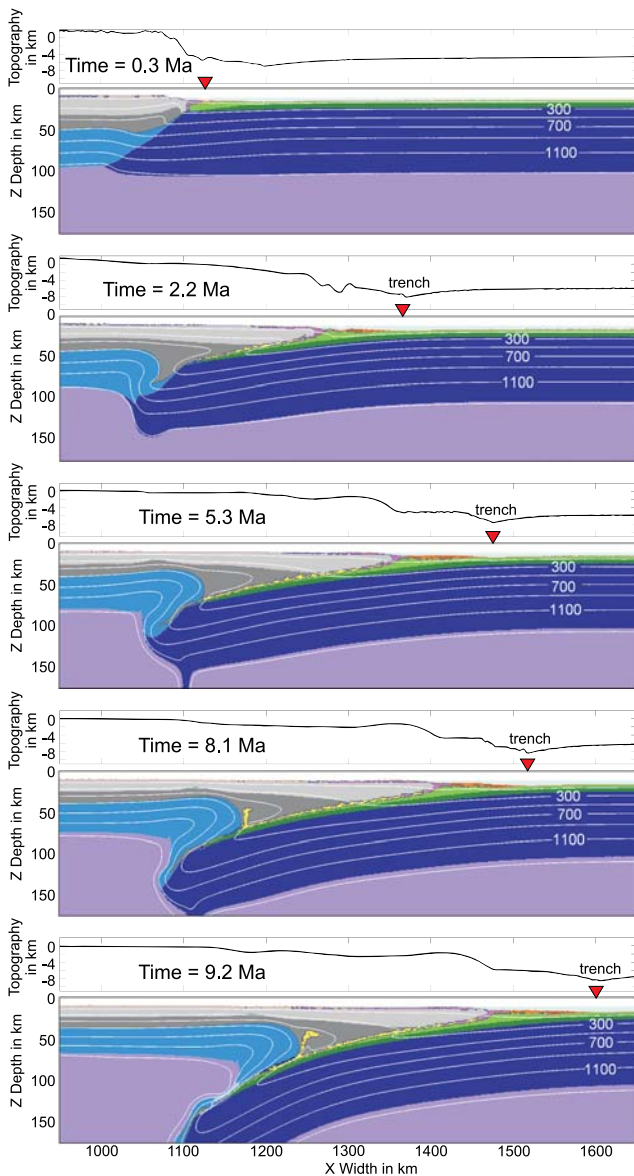


**Figure 13.** Influence of the plastic strength of the continental crust on the typical mode of subduction initiation (experiment 102). General development remains unchanged, but the time needed for lithospheric failure increases (compare with Figure 4).

continental crust over the oceanic one and related viscoplastic bending of the oceanic plate [Gerya and Yuen, 2007; Faccenda et al., 2008]. After initiation of subduction, this trench sustains (Figure 17b) owing to the growing load arising from the subducting slab. There is no undeniable difference in depth between trenches formed by overthrusting and subduction (Figures 3, 4, and 17). In the case of subduction initiation the transition from overthrusting stage to proper subduction is characterized by the period of trench depth relaxation associated with prolonged ductile shearing of the continental/oceanic lithospheric boundary (compare Figures 3 and 17b). Another remarkable topography feature is a frontal bulge formed at 100–300 km from

the trench landward. It is clearly observed in experiments with large ( $>150$  km) overthrusting as well as in experiments resulting in subduction initiation (Figures 3, 4, and 17), and its formation is related to deflection of the thinner

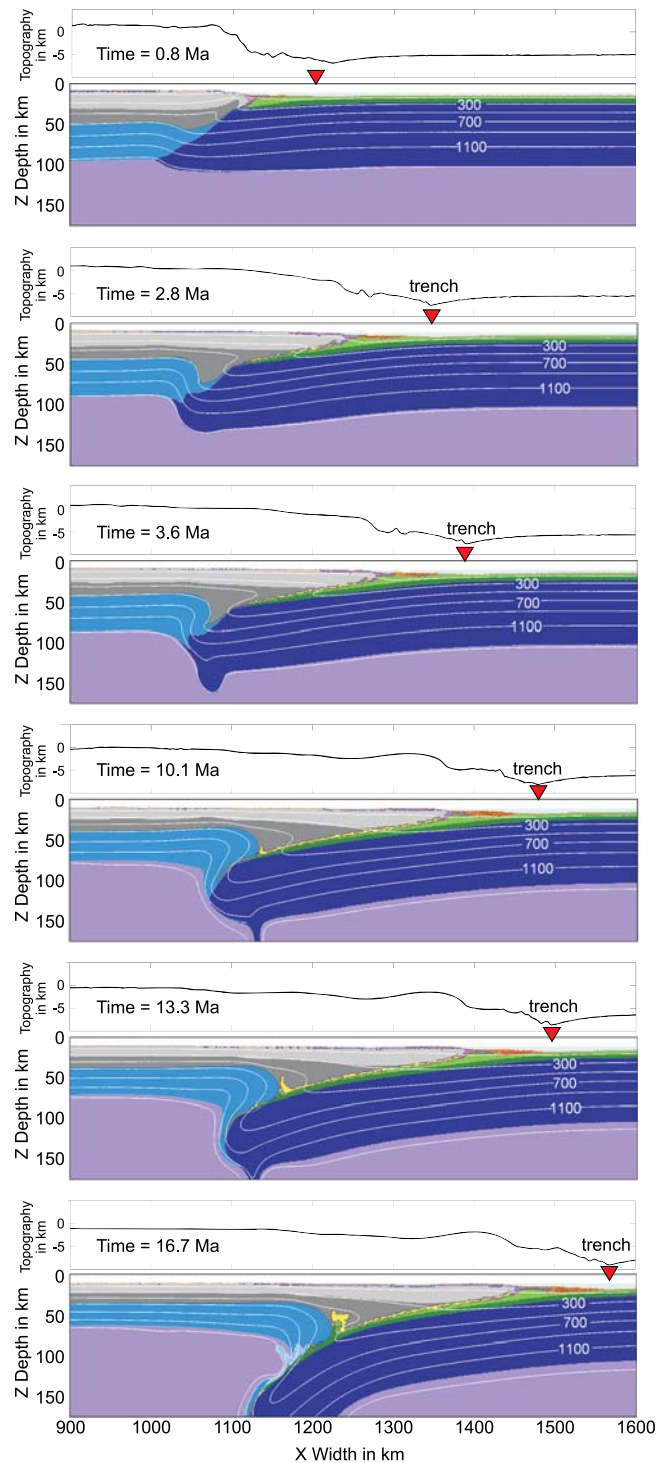


**Figure 14.** Influence of the plastic strength of the continental crust on the slow mode of subduction initiation (experiment 98). General development remains unchanged, but the time needed for lithospheric failure decreases (compare with Figure 5).

**Table 8.** Description of Numerical Experiments 116–125 With Varying Pore Fluid Pressure Factor of the Continental Crust<sup>a</sup>

Experiment	Pore Fluid Pressure Factor $\lambda$	Internal Friction $\cos(\varphi)$ of Hydrated Rocks <sup>b</sup>		Density Contrast (kg/m <sup>3</sup> )	Thickness of Continental Plate (km)	Geodynamic Regime	Time of Subduction Initiation (Ma)	Thrust Sheet Length (km)
		Continental Crust	Mantle					
10 <sup>c</sup>	1.0	0.0	0.0	25	90	subduction	2.7	...
116	0.75	0.025	0.05	25	90	subduction	5.0	...
117	0.7	0.03	0.06	25	90	subduction	5.8	...
118	0.6	0.04	0.08	25	90	subduction	7.6	...
119	0.5	0.05	0.1	25	90	subduction	10.0	...
12 <sup>c</sup>	1.0	0.0	0.0	25	110	overthrusting	...	250
120	0.95	0.005	0.01	25	110	stable margin	...	5
33 <sup>c</sup>	1.0	0.0	0.0	100	100	subduction	4.1	...
121	0.75	0.025	0.05	100	100	subduction	4.7	...
122	0.6	0.04	0.08	100	100	subduction	6.7	...
123	0.5	0.05	0.1	100	100	subduction	7.9	...
34 <sup>c</sup>	1.0	0.0	0.0	100	110	subduction	20.1	...
124	0.75	0.025	0.05	100	110	subduction	15.2	...
125	0.6	0.04	0.08	100	110	subduction	16.0	...

<sup>a</sup>The age of the oceanic plate is 40 Ma, thickness of the continental crust equals 44 km, and the internal friction of the continental crust is  $\sin(\varphi) = 0.1$ .

<sup>b</sup>Internal friction of hydrated rocks is calculated from friction coefficient of dry rocks and fluid pressure factor as  $\sin(\varphi) = \sin(\varphi_{dry})(1 - \lambda)$ .

<sup>c</sup>Experiments with zero friction at upper slab interface listed also in Table 4.

frontal part of the forming crustal sheet interacting with the bending oceanic plate.

[32] The experiments show that in the case of laterally uniform lithospheric thickness, the transition from over-

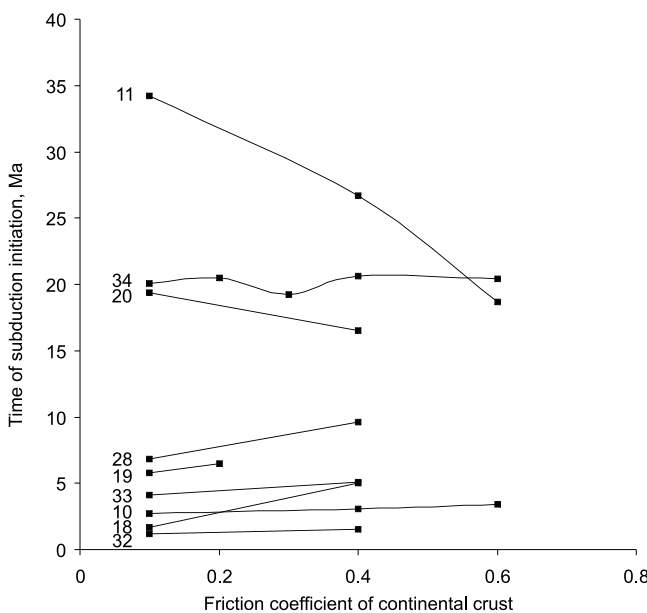


**Figure 15.** Time of subduction initiation as a function of the continental crust strength (see text for details). Number of the reference experiment with the  $\sin(\varphi) = 0.1$  is shown at the beginning of each curve. The increase in strength of the continental crust influences the time of subduction initiation differently depending on its mode: Experiments that showed a rather fast mode of subduction initiation (lower group of curves: experiments 32, 18, 10, 33, 19, and 28) are characterized by a slower evolution of subduction zone with increasing crustal strength. Experiments that showed a slow mode of subduction initiation (upper group of curves: experiments 11, 34, and 20) are characterized by a faster development of subduction zone with increasing strength of crustal rocks.

thrusting to subduction is not expressed in any specific topography features before subduction causes development of a back-arc basin and an oceanic arc. However, it is important to mention that topography development is strongly sensitive to the initial margin geometry and may differ for experiments with nonuniform lithospheric thickness.

**5. Conclusions**

[33] We investigated factors controlling the stability of passive margins, such as age of the oceanic plate, thickness of the continental lithosphere and crust, and density contrast between subcontinental and suboceanic lithospheric man-

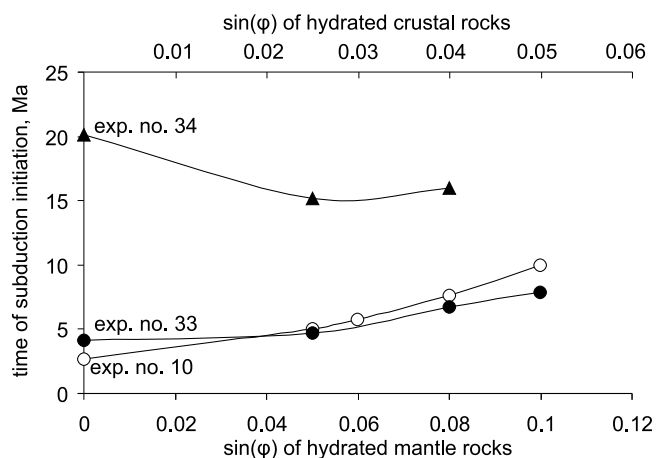


**Figure 16.** Time of subduction initiation as a function of the strength of hydrated rocks ( $\sin(\varphi)$  is shown for hydrated mantle and crustal rocks). Each curve is marked with the number of the reference experiment with the zero strength of hydrated rocks. Similarly to the effect of increasing strength of the continental crust (Figure 15), the increase in strength of the slab overlying rocks either decreases (slow mode) or increases (fast mode) the time of subduction initiation depending on the mode of the process.

**Table 9.** Description of Numerical Experiments 126–130 With Varying Sediment Loading<sup>a</sup>

Experiment	Density Contrast (kg/m <sup>3</sup> )	Thickness of Sediment		Geodynamic Regime	Time of Subduction Initiation (Ma)	Thrust Sheet Length (km)
		Continental Plate (km)	Loading (km)			
10	25	90	0	subduction	2.7	...
126	25	90	5	overthrusting	...	250
28	75	100	0	subduction	6.8	...
127	75	100	1	subduction	11.0	...
128	75	100	5	overthrusting	...	350
129	75	100	10	overthrusting	...	250
28	75	110	0	overthrusting	...	350
130	75	110	10	overthrusting	...	210

<sup>a</sup>The age of the oceanic plate is 40 Ma, thickness of the continental crust equals 44 km, and the internal friction of the continental crust is  $\sin(\varphi) = 0.1$ .

ties. The numerical experiments show the following: (1) Three subsequent tectonic regimes can be distinguished at a passive margin: stable margin, overthrusting, and subduction. (2) The stability of a passive margin depends on the strength of the continental lithosphere rather than on that of the oceanic one. (3) Transition from stable margin to the overthrusting regime is mainly controlled by ductile strength of the continental crust; however, other parameters such as density of the underlying lithospheric continental mantle and brittle/plastic strength of the upper continental crust affect thrust sheet length and thickness. (4) Transition from overthrusting to subduction initiation is mainly controlled by ductile strength and density of the continental lithosphere. (5) Age of the oceanic plate is a factor of secondary importance in subduction initiation: it plays a role if other parameters are of critical values.

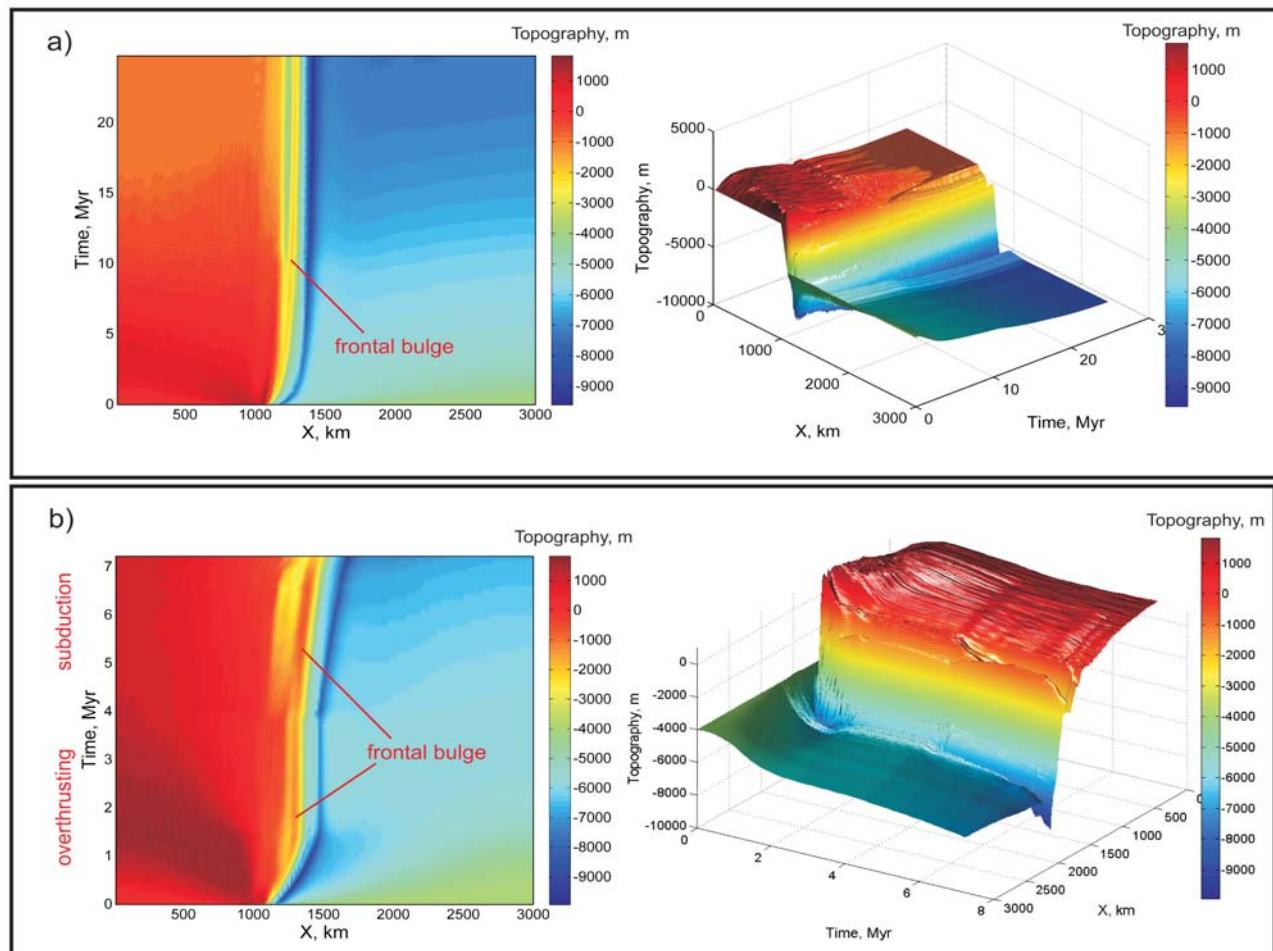


**Figure 17.** Topography evolution with time in experiments with (a) overthrusting regime and (b) subduction initiation. Corresponding evolution of lithological and temperature fields during these two experiments is shown in Figures 3 and 4, respectively. In both experiments the initial stage of development is characterized by creeping of the continental crust over the oceanic one and formation of an oceanic trench and a frontal bulge. In the case of the overthrusting tectonic regime, the model reaches steady state at ~18 Ma, whereas in the case of subduction, the period of inactivity in topography development (from ~1.5 to ~4 Ma) is followed by proper subduction [initiation accompanied by trench retreat and deepening and back-arc rifting.

[34] **Acknowledgments.** This work was supported by ETH research grants TH-12/05-3 and TH-0807-3, SNF research grants 200021-113672/1 and 200021-116381/1, and the RF President Program “Leading Scientific School of Russia” (grant 1949.2008.5) to T.V.G. F.O.M. acknowledges a sabbatical fellowship from FCT Portugal.

## References

- Behn, M. D., and P. B. Kelemen (2003), Relationship between seismic  $P$  wave velocity and the composition of anhydrous igneous and meta-igneous rocks, *Geochem. Geophys. Geosyst.*, *4*(5), 1041, doi:10.1029/2002GC000393.
- Brace, W. F., and D. L. Kohlstedt (1980), Limits on lithospheric stress imposed by laboratory experiments, *J. Geophys. Res.*, *85*, 6248–6252, doi:10.1029/JB085iB11p06248.
- Carlson, R. L. (2001), The abundance of ultramafic rocks in Atlantic Ocean crust, *Geophys. J. Int.*, *144*, 37–48.
- Carlson, R. W., D. G. Pearson, and D. E. James (2005), Physical, chemical, and chronological characteristics of continental mantle, *Rev. Geophys.*, *43*, RG1001, doi:10.1029/2004RG000156.
- Casey, J. F., and J. F. Dewey (1984), Initiation of subduction zones along transforms and accreting plate boundaries, triple junction evolution, and forearc spreading centers: Implications for ophiolitic geology and obduction, in *Ophiolites and Oceanic Lithosphere*, edited by I. G. Gass, S. J. Lippard, and A. W. Shelton, *Geol. Soc. Spec. Publ.*, *13*, 269–290.
- Clauser, C., and E. Huenges (1995), Thermal conductivity of rocks and minerals, in *Rock Physics and Phase Relations: A Handbook of Physical Constants, Ref. Shelf Ser.*, vol. 3, edited by T. J. Ahrens, pp. 105–126, AGU, Washington, D. C.
- Cloetingh, S. A. P. L., M. J. R. Wortel, and N. J. Vlaar (1982), Evolution of passive continental margins and initiation of subduction zones, *Nature*, *297*, 139–142, doi:10.1038/297139a0.
- Cloetingh, S. A. P. L., M. J. R. Wortel, and N. J. Vlaar (1984), Passive margin evolution, initiation of subduction and the Wilson cycle, *Tectonophysics*, *109*, 147–163, doi:10.1016/0040-1951(84)90175-6.
- Cloetingh, S. A. P. L., M. J. R. Wortel, and N. J. Vlaar (1989), On the initiation of subduction zones, *Pure Appl. Geophys.*, *129*, 7–25, doi:10.1007/BF00874622.
- Cloos, M. (1993), Lithospheric buoyancy and collisional orogenesis: Subduction of oceanic plateaus, continental margins, island arcs, spreading ridges, and seamounts, *Geol. Soc. Am. Bull.*, *105*, 715–737, doi:10.1130/0016-7606(1993)105<0715:LBACOS>2.3.CO;2.
- Connolly, J. A. D. (2005), Computation of phase equilibria by linear programming: A tool for geodynamic modelling and its application to subduction zone decarbonation, *Earth Planet. Sci. Lett.*, *236*, 524–541, doi:10.1016/j.epsl.2005.04.033.
- Davies, G. F. (1999), *Dynamic Earth*, Cambridge Univ. Press, New York.
- Davies, J. H. (1999), The role of hydraulic fractures in generating intermediate depth earthquakes and subduction zone magmatism, *Nature*, *398*, 142–145, doi:10.1038/18202.
- Deen, T. J., W. L. Griffin, G. Begg, S. Y. O’Reilly, L. M. Natapov, and J. Hronsky (2006), Thermal and compositional structure of the subcontinental lithospheric mantle: Derivation from shear wave seismic tomography, *Geochem. Geophys. Geosyst.*, *7*, Q07003, doi:10.1029/2005GC001120.
- Dewey, J. F. (1969), Continental margins: A model for conversion of Atlantic type to Andean type, *Earth Planet. Sci. Lett.*, *6*, 189–197, doi:10.1016/0012-821X(69)90089-2.
- Dickinson, W. R., and D. R. Seely (1979), Structure and stratigraphy of fore-arc regions, *Am. Assoc. Pet. Geol. Bull.*, *63*, 2–31.
- Doin, M.-P., and P. Henry (2001), Subduction initiation and continental crust recycling: The roles of rheology and eclogitization, *Tectonophysics*, *342*, 163–191, doi:10.1016/S0040-1951(01)00161-5.
- Eldholm, O., and M. F. Coffin (2000), Large igneous provinces and plate tectonics, in *The History and Dynamics of Global Plate Motions, Geophys. Monogr. Ser.*, vol. 121, edited by M. A. Richards, R. G. Gordon, and R. van der Hilst, pp. 309–326, AGU, Washington, D. C.
- Erickson, S. G. (1993), Sedimentary loading, lithospheric flexure, and subduction initiation at passive margins, *Geology*, *21*, 125–128, doi:10.1130/0091-7613(1993)021<125:SLLFAS>2.3.CO;2.
- Faccenda, M., L. Burlini, T. V. Gerya, and D. Mainprice (2008), Fault-induced seismic anisotropy by hydration in subducting oceanic plates, *Nature*, *455*, 1097–1100, doi:10.1038/nature07376.
- Fyfe, W. S., and O. H. Leonardos (1977), Speculations on causes of crustal rifting and subduction, with applications to the Atlantic margin of Brazil, *Tectonophysics*, *42*, 29–36, doi:10.1016/0040-1951(77)90015-4.
- Gerya, T. V., and D. A. Yuen (2007), Robust characteristics method for modelling multiphase visco-elasto-plastic thermo-mechanical problems, *Phys. Earth Planet. Inter.*, *163*, 83–105, doi:10.1016/j.pepi.2007.04.015.
- Gerya, T. V., A. D. Connolly, D. A. Yuen, W. Gorczyk, and A. M. Capel (2006), Seismic implications of mantle wedge plumes, *Phys. Earth Planet. Inter.*, *156*, 59–74, doi:10.1016/j.pepi.2006.02.005.
- Gerya, T. V., J. A. D. Connolly, and D. A. Yuen (2008), Why is terrestrial subduction one-sided?, *Geology*, *36*, 43–46, doi:10.1130/G24060A.1.
- Gorczyk, W., A. P. Willner, J. A. D. Connolly, and J.-P. Burg (2007), Physical controls of magmatic productivity at Pacific-type convergent margins: New insights from numerical modeling, *Phys. Earth Planet. Inter.*, *163*, 209–232, doi:10.1016/j.pepi.2007.05.010.
- Goren, L., E. Aharonov, G. Mulugeta, H. A. Koyi, and Y. Mart (2008), Ductile deformation of passive margins: A new mechanism for subduction initiation, *J. Geophys. Res.*, *113*, B08411, doi:10.1029/2005JB004179.
- Gurnis, M., C. Hall, and L. Lavier (2004), Evolving force balance during incipient subduction, *Geochem. Geophys. Geosyst.*, *5*, Q07001, doi:10.1029/2003GC000681.
- Hall, C., M. Gurnis, M. Sdrolias, L. L. Lavier, and R. D. Müller (2003), Catastrophic initiation of subduction following forced convergence across fracture zones, *Earth Planet. Sci. Lett.*, *212*, 15–30, doi:10.1016/S0012-821X(03)00242-5.
- Hilde, T. W. E., S. Uyeda, and L. Kroenke (1977), Evolution of the western Pacific and its margin, *Tectonophysics*, *38*, 145–165, doi:10.1016/0040-1951(77)90205-0.
- Jordan, T. H. (1978), Composition and development of the continental tectosphere, *Nature*, *274*, 544–548, doi:10.1038/274544a0.
- Karig, D. E. (1982), Initiation of subduction zones: Implications for arc evolution and ophiolite development, *Geol. Soc. Spec. Publ.*, *10*, 563–576, doi:10.1144/GSL.SP.1982.010.01.37.
- Karson, J., and J. F. Dewey (1978), Coastal Complex, western Newfoundland: An early Ordovician oceanic fracture zone, *Geol. Soc. Am. Bull.*, *89*, 1037–1049, doi:10.1130/0016-7606(1978)89<1037:CCWNAE>2.0.CO;2.
- Kemp, D. V., and D. J. Stevenson (1996), A tensile, flexural model for the initiation of subduction, *Geophys. J. Int.*, *125*, 73–94, doi:10.1111/j.1365-246X.1996.tb06535.x.
- Lallemand, S., Y. Font, H. Bijwaard, and H. Kao (2001), New insights on 3-D plates interaction near Taiwan from tomography and tectonic implications, *Tectonophysics*, *335*, 229–253, doi:10.1016/S0040-1951(01)00071-3.
- Lee, C., Q. Yin, R. L. Rudnick, and S. B. Jacobsen (2001), Preservation of ancient and fertile lithospheric mantle beneath the southwestern United States, *Nature*, *411*, 69–73, doi:10.1038/35075048.
- Mart, Y., E. Aharonov, G. Mulugeta, W. Ryan, T. Tentler, and L. Goren (2005), Analogue modelling of the initiation of subduction, *Geophys. J. Int.*, *160*, 1081–1091, doi:10.1111/j.1365-246X.2005.02544.x.
- McKenzie, D. P. (1977), The initiation of trenches: A finite amplitude instability, in *Island Arcs, Deep Sea Trenches, and Back-Arc Basins, Maurice Ewing Ser.*, vol. 1, edited by M. Talwani and W. C. Pitman III, pp. 57–61, AGU, Washington, D. C.
- Mitchell, A. H. G. (1984), Initiation of subduction of post-collision foreland thrusting and back-thrusting, *J. Geodyn.*, *1*, 103–120, doi:10.1016/0264-3707(84)90023-1.
- Moore, D. E., D. A. Lockner, M. Shengli, R. Summers, and J. D. Byerlee (1997), Strengths of serpentinite gouges at elevated temperatures, *J. Geophys. Res.*, *102*, 14,787–14,801, doi:10.1029/97JB00995.
- Morris, J. D., and S. R. Hart (1986), Isotopic and incompatible element constraints on the genesis of island-arc volcanics from Cold Bay and Amak Island, Aleutians, and implications for mantle structure—Reply, *Geochim. Cosmoch. Acta*, *50*, 483–487.
- Müller, S., and R. J. Phillips (1991), On the initiation of subduction, *J. Geophys. Res.*, *96*, 651–665, doi:10.1029/90JB02237.
- Nikolaeva, K. M., T. V. Gerya, and J. A. D. Connolly (2008), Numerical modeling of crustal growth in intraoceanic volcanic arcs, *Phys. Earth Planet. Inter.*, *171*, 336–356, doi:10.1016/j.pepi.2008.06.026.
- Niu, Y., M. J. O’Hara, and J. A. Pearce (2003), Initiation of subduction zones as a consequence of lateral compositional buoyancy contrast within the lithosphere: A petrological perspective, *J. Petrol.*, *44*(5), 851–866, doi:10.1093/petrology/44.5.851.
- O’Reilly, S. Y., and W. L. Griffin (2006), Imaging global chemical and thermal heterogeneity in the subcontinental lithospheric mantle with garnets and xenoliths: Geophysical implications, *Tectonophysics*, *416*, 289–309, doi:10.1016/j.tecto.2005.11.014.
- Oxburgh, E. R., and E. M. Parmentier (1977), Compositional and density stratification in oceanic lithosphere: Causes and consequences, *J. Geol. Soc.*, *133*, 343–355, doi:10.1144/gsjgs.133.4.0343.
- Parsons, B., and J. G. Sclater (1977), An analysis of the variation of ocean floor bathymetry and heat flow with age, *J. Geophys. Res.*, *82*, 803–827, doi:10.1029/JB082i005p0803.

- Pascal, C., and S. A. P. L. Cloetingh (2009), Gravitational potential stresses and stress field of passive continental margins: Insights from the south-Norway shelf, *Earth Planet. Sci. Lett.*, *277*, 464–473, doi:10.1016/j.epsl.2008.11.014.
- Plank, T., and C. H. Langmuir (1998), The chemical composition of subducting sediment and its consequences for the crust and mantle, *Chem. Geol.*, *145*, 325–394.
- Poudjom Djomani, Y. H., S. Y. O'Reilly, W. L. Griffin, and P. Morgan (2001), The density structure of subcontinental lithosphere through time, *Earth Planet. Sci. Lett.*, *184*, 605–621, doi:10.1016/S0012-821X(00)00362-9.
- Ranalli, G. (1995), *Rheology of the Earth*, Chapman and Hall, London.
- Regenauer-Lieb, K., D. A. Yuen, and J. Branlund (2001), The initiation of subduction: Critically by addition of water?, *Science*, *294*, 578–580, doi:10.1126/science.1063891.
- Sankaran, A. V. (2001), Stability of ancient cratons and lithospheric mantle composition, *Curr. Sci.*, *81*, 1158–1160.
- Schmeling, H., et al. (2008), A benchmark comparison of spontaneous subduction models: Towards a free surface, *Phys. Earth Planet. Inter.*, *171*, 198–223, doi:10.1016/j.pepi.2008.06.028.
- Sobolev, S. V., and A. Y. Babeyko (2005), What drives orogeny in the Andes?, *Geology*, *33*, 617–620, doi:10.1130/G21557.1.
- Sobolev, S. V., H. Zeyen, M. Granet, U. Achauer, C. Bauer, F. Werling, R. Altherr, and K. Fuchs (1997), Upper mantle temperatures and lithosphere-asthenosphere system beneath the French Massif Central constrained by seismic, gravity, petrologic and thermal observations, *Tectonophysics*, *275*, 143–164, doi:10.1016/S0040-1951(97)00019-X.
- Solomatov, V. S. (2004), Initiation of subduction by small-scale convection, *J. Geophys. Res.*, *109*, B05408, doi:10.1029/2004JB003143.
- Staudigel, H., S. Hart, H. Schmincke, and B. Smith (1989), Cretaceous ocean crust at DSDP sites 417–418: Carbon uptake from weathering versus loss by magmatic outgassing, *Geochim. Cosmoch. Acta*, *53*, 3091–3094.
- Steckler, M. S., and U. S. ten Brink (1986), Lithospheric strength variations as a control on new plate boundaries: Examples from the northern Red Sea region, *Earth Planet. Sci. Lett.*, *79*, 120–132, doi:10.1016/0012-821X(86)90045-2.
- Stern, R. J. (2002), Subduction zones, *Rev. Geophys.*, *40*(4), 1012, doi:10.1029/2001RG000108.
- Stern, R. J. (2004), Subduction initiation: Spontaneous and induced, *Earth Planet. Sci. Lett.*, *226*, 275–292.
- Toth, J., and M. Gurnis (1998), Dynamics of subduction initiation at pre-existing fault zones, *J. Geophys. Res.*, *103*, 18,053–18,067, doi:10.1029/98JB01076.
- Turcotte, D. L., and G. Schubert (2002), *Geodynamics*, 456 pp., Cambridge Univ. Press, New York.
- Turcotte, D. L., W. F. Haxby, and J. R. Ockendon (1977), Lithospheric instabilities, in *Island Arcs, Deep Sea Trenches, and Back-Arc Basins, Maurice Ewing Ser.*, vol. 1, edited by M. Talwani and W. C. Pittman III, pp. 63–69, AGU, Washington, D.C.
- Ueda, K., T. Gerya, and S. V. Sobolev (2008), Subduction initiation by thermal-chemical plumes: Numerical studies, *Phys. Earth Planet. Inter.*, *171*, 296–312, doi:10.1016/j.pepi.2008.06.032.
- Uyeda, S., and Z. Ben-Avraham (1972), Origin and development of the Philippine Sea, *Nature*, *240*, 176–178.
- Van der Lee, S., K. Regenauer-Lieb, and D. A. Yuen (2008), The role of water in connecting past and future episodes of subduction, *Earth Planet. Sci. Lett.*, *273*, 15–27, doi:10.1016/j.epsl.2008.04.041.
- Vlaar, N. J., and M. J. R. Wortel (1976), Lithospheric aging, instability and subduction, *Tectonophysics*, *32*, 331–351, doi:10.1016/0040-1951(76)90068-8.
- Whitmarsh, R. B., G. Manatschal, and T. A. Minshull (2001), Evolution of magma-poor continental margins from rifting to seafloor spreading, *Nature*, *413*, 150–154, doi:10.1038/35093085.

T. V. Gerya and K. Nikolaeva, Department of Geosciences, Swiss Federal Institute of Technology, Sonneggstrasse 5, CH-8092 Zurich, Switzerland. (nikolaeva@erdw.ethz.ch)

F. O. Marques, Departamento Geologia, Faculdade Ciências, Universidade de Lisboa, P-1749-016 Lisbon, Portugal.